

1-1-2016

Kinematic Modeling Of An Automated Laser Line Scanning System

Kiran Sunil Deshmukh
Wayne State University,

Follow this and additional works at: http://digitalcommons.wayne.edu/oa_theses

 Part of the [Industrial Engineering Commons](#), and the [Robotics Commons](#)

Recommended Citation

Deshmukh, Kiran Sunil, "Kinematic Modeling Of An Automated Laser Line Scanning System" (2016). *Wayne State University Theses*. Paper 471.

This Open Access Thesis is brought to you for free and open access by DigitalCommons@WayneState. It has been accepted for inclusion in Wayne State University Theses by an authorized administrator of DigitalCommons@WayneState.

KINEMATIC MODELING OF AN AUTOMATED LASER LINE SCANNING SYSTEM

by

KIRAN SUNIL DESHMUKH

THESIS

Submitted to the Graduate School

of Wayne State University,

Detroit, Michigan

in partial fulfillment of the requirements

for the degree of

MASTER OF SCIENCE

2016

MAJOR: ENGINEERING MANAGEMENT

Approved By:

Advisor

Date

©COPYRIGHT BY
KIRAN SUNIL DESHMUKH
2016
All Rights Reserved

DEDICATION

This dissertation is gratefully dedicated to my loving father, Mr. Sunil Deshmukh, for earning an honest living for us and for supporting and encouraging me to believe in myself.

ACKNOWLEDGEMENTS

I would like to take this opportunity to thank all those who were part of fulfilling this thesis and research successfully. I would like to thank my advisor, Dr. Jeremy L. Rickli, for his continued support and guidance, and in showing me the correct path. Dr. Rickli has been invaluable throughout the duration of my thesis as well as an excellent advisor. He encouraged me to take leadership on this project as well as discover new approaches.

I would also like to express my gratitude to my co-advisor, Dr. Ana Djuric, for her support and excellent guidance in the kinematics modelling approach. She encouraged me to solve an approach in step by step manner and motivated my spirits to keep going. Also, I would like to thank my committee member, Dr. Evrim Dalkiran, for encouraging and supporting my research work.

Last, I would like to express my gratitude towards the faculty and staff of the Industrial & Systems Engineering Department and the Division of Engineering Technology who have helped me to complete my Master's Thesis. Finally, I am extremely thankful to my father, sisters, grandmother, and friends for trusting and supporting me throughout my work.

TABLE OF CONTENTS

DEDICATION	ii
ACKNOWLEDGEMENTS	iii
TABLE OF CONTENTS	iv
LIST OF FIGURES	v
LIST OF TABLES	vii
EXECUTIVE SUMMARY	viii
1. INTRODUCTION	1
2. LITERATURE REVIEW	5
3. ELEMENTS OF ALLS SYSTEM.....	14
4. MODELING OF ALLS SYSTEM	18
5. VALIDATION RESULTS FOR THE ALLS SYSTEM.....	35
5.1 Validation of Forward Kinematics for ALLS System	35
5.2 Spherical Component Surface.....	38
5.3 ALLS System Relative to Component.....	39
6. SCAN PATH EXPERIMENT & RESULTS	41
7. CONCLUSIONS AND FUTURE WORK	49
APPENDIX A	51
APPENDIX B	54
APPENDIX C	55
APPENDIX D	60
REFERENCES	61
ABSTRACT.....	68
AUTOBIOGRAPHICAL STATEMENT.....	69

LIST OF FIGURES

Figure 1: Pictorial representation of this thesis statement	3
Figure 2: Integrated 3D scanning system (Yin, Ren et al. 2014).....	10
Figure 3: Relationship between the scanning frame and robot frame (Yin et al. 2014).....	11
Figure 4: Kinematics of robot-base, tool, and surface for a wire embedding process (Kim et al. 2015).	12
Figure 5: Laser line scanner parameters (Bračun, Jezeršek et al. 2006).....	15
Figure 6: FANUC S430 IW robot with MetraSCAN-R 3D laser scanner attached as end-effector	16
Figure 7: Offset of the Creaform MetraSCAN-R laser line scanner (MetraSCAN AutoCad file).....	16
Figure 8: System components of an ALLS system	17
Figure 9: Kinematic model structure of measurement of point cloud system-FANUCS430 IW, Metra Scan 3D scanner, and beam, addition to the Arachchige et al. (2014) model.....	20
Figure 10: Position vector p for spherical wrist robots (Odeyinka 2015).....	23
Figure 11: Projection of vector p onto $x_0- y_0$ for Joint 1 (Odeyinka and Djuric 2016)	25
Figure 12: Projection of vector p onto $x_1- y_1$ for Joint 2 (Odeyinka and Djuric 2016).....	26
Figure 13: Projection of vector p onto $x_2- y_2$ for Joint 3 (Odeyinka and Djuric 2016).....	28
Figure 14: Rotation about joint five (Odeyinka and Djuric 2016).....	30
Figure 15: Rotation about joint five for joint 4 (Odeyinka and Djuric 2016).....	32
Figure 16: Rotation about joint five for joint six (Odeyinka and Djuric 2016).....	33
Figure 17: Validation of FANUC Robot S-430 IW model.....	36
Figure 18: Validation result of the laser scanner and robot model.....	37
Figure 19: Validation result of the ALLS system.....	38
Figure 20: Validation result shows plotted equation of spherical component surface	39
Figure 21: Inverse Kinematics validation at $\theta_1, \theta_2, \theta_3, \theta_4, \theta_6 = 0; \theta_5 = -90$	40
Figure 22: System movement position on the point of trajectory of component surface extension	40
Figure 23: Master-calibration step on Teach Pendant of FANUC S-430 IW robot	42

Figure 24: Single Axis Master on Teach Pendant of FANUC S-430 IW robot	42
Figure 25: Calibrate on Teach Pendant of FANUC S-430 IW robot.....	43
Figure 26: Jogging the unmastered Axis of all Joints J ₁ to J ₆ axis of FANUC S-430 IW robot using Teach Pendant	43
Figure 27: Setting safety limit on FANUC S-430 IW robot.....	44
Figure 28: Setting the tool frame on the FANUC S-430 IW robot.....	45
Figure 29: Scanner calibration is controlled using FANUC S430 IW robot and determined scanner position and orientation	46
Figure 30: Scanning of Spherical surface: the position of point co-ordinates on the spherical surface and joint angles of FANUC S-430 IW robot and scanner to reach the surface.	48
Figure 31: FANUC S430 IW Robot and MetraSCAN-R system two poses (pink dots) while scanning a trajectory points on component surface	48

LIST OF TABLES

Table 1: Summary of literature review: explaining gap analysis and my thesis.....	13
Table 2: D-H parameters for FANUC S430 IW, MetraSCAN-R scanner and beam (Arachchige et al. 2014)	19
Table 3: Different possible arm configurations for joint three (Odeyinka and Djuric 2016)	29
Table 4: Elements or column of Resultant Matrix q_1	32
Table 5: Elements of Resultant Matrix q_2	34

EXECUTIVE SUMMARY

Several studies have focused on collecting the information of worn out, broken and repaired surfaces of components in manufacturing and remanufacturing processes (Papaioannou, Karabassi et al. 2002; Zhu, Guo et al. 2005; Jin and Yang 2009; Haapala, Zhao et al. 2013; Rickli, Dasgupta et al. 2014; Chen, Wang et al. 2014). This research aims to solve the problem of path planning, data capturing and point cloud datasets using an automated laser line scanning system; however, there has been little research integrating the three frame; robot, laser scanner and component surface. The goal of this work is to link the automated laser line scanning system with the component surface and establish the fundamental kinematic models required for advanced automated scan path planning. The study of these linkages provides the knowledge of the transformation of geometric Cartesian coordinates in a given measurement system. This knowledge is necessary for advanced planning of a scan path for a component. With this model, it is possible to determine, the position and orientation of a robot arm, laser scanner, laser beam, and component with respect to the robot base during its movement along a trajectory to collect points on the component surface. The goal of this trajectory path is intended to act as an input for optimization routines, which converge to the scan path, which acquires the best point cloud data, for quality monitoring in manufacturing and core condition assessment in remanufacturing.

To solve this problem, our approach is by doing the following: (i) Solving the forward kinematics of a six degree of freedom robot, laser scanner and laser beam (ii) Deriving the equation for a component surface, and (iii) Modifying the inverse kinematics for the robot-scanner system to move along a point on the component surface. The inverse kinematics equations determine the orientation of the robot joint angles relative to the component surface.

System equations are validated using Matlab, simulation model Workspace LT, and on FANUC S-430 IW robot and MetraSCAN-R system using Teach Pendant programming. The scanning of a spherical surface experiment is performed to validate the scanning movement along the trajectory path, and the joint angles are recorded during the scanning motion. The contribution and intellectual merit of this research is the continuous geometric transformation from the robot, the scanner, and the beam to a point on the component surface.

With this model, it is possible to determine the position and orientation of a robot arm, laser scanner, laser beam, and component with respect to the robot base during its movement along a trajectory to collect points on the component surface. The obtained position and orientation of the robot-laser scanning system is critical to future work to develop the work-window for the FANUC S-430 IW robot and MetraSCAN-R scanning system.

1. INTRODUCTION

The geometric coordinate changes between the elements of automated laser scanning system when an automated laser line scanning system (e.g. for component inspection in manufacturing and remanufacturing processes) scans along a path of a component surface are yet to be fully determined and modeled. In today's manufacturing world, the increase in complex specifications and zero defects as well as the focus on high quality for components has gained much attention, which has created a need for and willingness, to enhance inspection systems. In inspection systems, methods such as coordinate measuring machines make physical contact with each point on a surface and, thus, can be slow in acquiring component surface data (Lee and Park 2000). Laser line scanners, on the other hand, can obtain large amounts of data with a high resolution of digitization and inspection (Xi and Shu 1999; Kuş 2009) in a shorter period of time, as compared to contact type methods (Lee and Park, 2000; Son et al. 2002; Yin et al. 2014). The need for development of automated laser scanning system models is to avoid the trial and error caused by manual scanning (Son et al. 2002; Borangiu, Dogar et al. 2009;), increase the information content from as-manufactured components for the digital thread, and improve the effectiveness of scanned data.

An Automated Laser Line Scanning System (ALLS) is composed of four basic components: (i) a six degree of freedom robot arm (Pieper 1968, Denavit and Hartenberg 1955, Vincze et al. 1994, Shen and Zhu 2012, Larsson and Kjellander 2006) or a modified coordinate measuring machine (Yau and Menq, 1995); (ii) a laser line scanner or a scanning probe; (iii) a component surface, sometimes placed on a turntable (Reinhart and Tekouo, 2009) or a rotary table (Shen and Zhu, 2012, Larsson and Kjellander, 2006) or fixed at a point; and (iv) a control system with algorithms for scan path planning based on scan parameters (Lee and Park 2000; Bračun et

al. 2006). In an ALLS system a scan path is planned for each surface of a part (Larsson and Kjellander 2008); consequently, the points are collected along that path. These collected points are recorded as measured points in point cloud data, which are further analyzed to compare geometry and develop CAD models (Pauly et al. 2004; Triebel et al. 2004). Each measured point on a component surface corresponds to a certain position and orientation of system elements (Yau and Menq 1995). Jin and Yang (2009) developed an algorithm using a CAD model for a laser remanufacturing robot system, in which the end-effector position and orientation control the movement of the scanner for shape measurement to reconstruct the surface. As a result, both Yau and Menq (1995) and Jin and Yang (2009) provided the motivation for this research to understand the geometric transformation of coordinates in the robot scanning system in relation to the component surface in manufacturing processes (Rickli.et.al. 2014).

There has been considerable research on automated scanning systems on motion control during data capturing, path planning strategies, and point cloud datasets of the dimensional data of component surface (Larsson and Kjellander 2006; Larsson and Kjellander 2008; Pauly et al. 2004). However, to the best of our knowledge, none have yet fully solved the complete kinematic relationship between the robot base and the laser scanner (Shen and Zhu 2012) without an external device (Yin et al. 2014) and addressing the relationship between a tool and component surface (Kim et al. 2015). Although the non-contact type of inspection system acquires ‘as-is’ component surface data by employing various efficient scanning methods and analyzing point cloud data, the kinematic relationship between the robot, scanner, and fixed component surface, as shown in Figure 1, without an external measuring device is to be fully determined.

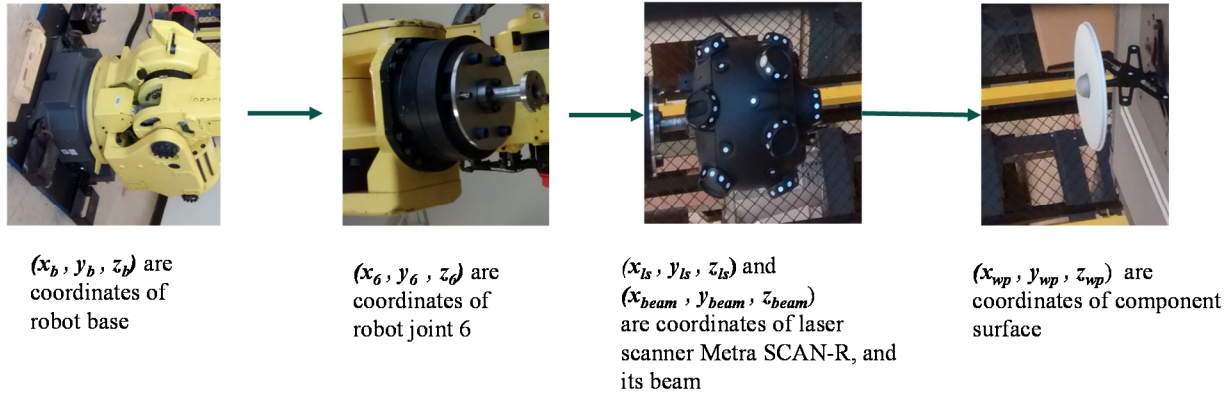


Figure 1: Pictorial representation of this thesis statement

The objective of this thesis is to integrate three co-ordinate frames; the robot, scanner, and component while scanning a trajectory path (scan path). This integration as shown in Figure 1, mathematically links the ALLS system with the component surface in order to establish the fundamental kinematic models required for automated laser line scanning of a component surface. The analysis of these mechanical linkages provides insight into the transformation of geometric Cartesian coordinates in a given measurement system. This knowledge is necessary for advanced planning of a scan path on a component. With this model, it is possible to determine the position and orientation of the robot arm, laser scanner, laser beam, and component with respect to the robot base during its movement along a trajectory to collect scanned points on the surface of a component. To achieve this research objective, the proposed approach is to solve the forward kinematics between the robot, laser scanner and component, use inverse kinematics, and move the system to the component coordinate points (Arachchige et al. 2014; Odeyinka and Djuric 2016). Using this set of equations will enable the determination of the position and orientation angles for each robot joint.

The remainder of this thesis is organized in the following manner: chapter 2 explains the literature review, chapter 3 describes the elements of an ALLS system, chapter 4 explores the modelling approach of the ALLS system, chapter 5 states the validation results of the model, chapter 6 mentions about the scanning experiment to obtain trajectory scan path, and the last chapter 7 describes conclusions drawn from the generated model as well as the future scope of this work.

2. LITERATURE REVIEW

A scan path is a continuous geometric description of the movement of a scanner controlled by robot (Larsson and Kjellander 2006). This research focuses on the geometric transformation in the system with respect to the component surface. It provides an opportunity to enhance scan path planning by calculating the positions of the robot arm, scanner, and beam while scanning along a defined trajectory on a component and observing that point coordinates are changing continuously along that trajectory path. Previous research has been done on developing algorithms to determine robot pose relative to component surface (Jin and Yang 2009), the kinematic relationship between the tool and component surface using three degree of freedom prismatic machine (Kim et al. 2015) and the relation between a six degree of freedom robot and laser scanner with and without an external tracking device (Vincze et al., 1994; Larsson and Kjellander 2006; Larsson and Kjellander 2008; Shen and Zhu 2012; Yin et al. 2014).

The scan path consists of a series of the predetermined line segments during the scanning of component surfaces (Son et.al. 2002). A laser line scanner acquires 3D coordinates of the component surfaces through image processing and the laser triangulation. When the image is captured, the system automatically finds the optical focus and maintains a stand-off distance. The length of the laser stripe and the stand-off distance is the distance of the laser beam focused on the component surface, and it is assumed constant in this research (Son, Park et.al 2002). The scanning process is critical to an inspection system because it can be time consuming due to no active control on scanning coverage, resulting in excessive or under scanning of surfaces (Kriegel, Bodenmüller et al. 2011; Xi and Shu 1999). An ALLS system controlled by a six degree of freedom robot (Larsson and Kjellander 2006) captures the component surfaces without manual intervention in the form of point cloud datasets while scanning along a pre-programmed path with pre-determined

scan parameters. These scan parameters are selected based on the component surface and inspection objectives. An ALLS system research has focused on problems of data capturing (Larsson and Kjellander 2006), scan path planning strategies (Larsson and Kjellander 2008), and analysis of point cloud datasets (Pauly et al. 2004; Lu and Milios 1997; Beringia et al. 2009) but focus on the scan points on the component surface corresponds to the position and orientation of the robot-scanning system is less explored. Hence, it has turned the attention of researchers to determine the kinematic relationship between the robot frame and the laser frame.

2.1 Data capturing problem

An automatic scanning system captures the “as- is” data of the part surface, and the scanning result is a point cloud, which is in a triangular mesh or point form (Surmann, Nüchter et al. 2003; Stamos and Leordean 2003). The quality of this ‘as-is’ point cloud data depends on the maximum number of points collected while scanning the path. Component surface data is captured by planning a scan path along a component surface. In Larsson & Kjellander (2006) ALLS system, a laser scanner is mounted on a robot in combination with a turntable, and it is moved along a scan path. Consequently, it becomes important to know the relation between the robot poses in relation to the component surface. The robot poses are defined as the robot-scanner moves to view the object from different positions while the scanner scans the component surface. The component surface is rotated using a turntable (Larsson and Kjellander 2006), and a robot moves the scanner to view the surface from different angles using camera. Hence, during data capturing it is necessary to know the rotation angle of the turntable with respect to the robot position in order to move the robot.

2.2 Scan path planning strategies

The focus of previous work regarding scan path planning has included different scan path planning strategies, an algorithm to generate a scan path using the CAD model (Jin and Yang 2009), laser line scanner parameters that affect the scan path (ElMaraghy and Yang 2003), and a path or view planning method to orient the measuring system relative to the object in each individual scan (Larsson and Kjellander 2008). Different scan path planning strategies intending to improve the quality of scan data are done by: (i) interpreting geometrical data measured directly from surface of existing objects, (ii) breaking broken regions into layers of worn out parts (Wu and Hu 2012), (iii) direct slicing to obtain path data on curved surface (Xi and Shu 1999; Bračun et al. 2006; Mehdi-Souzani, Thiébaud et al. 2006; Fernández, Rico et al. 2008; Jin and Yang 2009; Larsson and Kjellander 2008), and on existing objects with predefined scan patterns (ElMaraghy and Yang 2003). To implement different scan path planning methodologies with an ALLS system, we need to first understand the transformation in geometric coordinates during scanning given a component surface.

2.3 Analysis of point cloud datasets

Point cloud datasets are obtained from a scanned component surface (Derigent, Chapotot et al. 2007; Durupt, Remy et al. 2008). Due to cumbersome scanning procedures, problems of inconsistencies, uncertainty, and variations are observed in point cloud data. There are different methods to solve the uncertainty and variation in a point cloud by analyzing these datasets in various forms to extract high level information about scanned objects and to create renditions meaningful to a user by modifying the shape or appearance of point cloud data (Pauly et al. 2004). A study by Lu and Milios (1997) attempted to solve the problem of inconsistency in point cloud datasets by collecting and estimating two scans from two different robot poses. While scanning is

done, the two scans are aligned and matched (Borangi et al. 2009). An alternative approach addressed in this thesis is to focus on understanding the fundamental changes in the kinematic structure of an automated laser scanning system based on its relative position and orientation while moving on the trajectory of a component surface. The quality of the point cloud depends on the closeness to measured points along a scan path. This collection of closely measured points on a scan path has gathered importance in manufacturing, reverse engineering and remanufacturing due to growing interest in advanced inspection systems, the model based enterprise and the product or manufacturing digital thread (Rickli et al. 2014). This shifts the focus from analyzing point cloud segments (Triebel et al. 2004) to studying the occurrence of the geometric transformation of point coordinates while scanning surfaces or moving along a trajectory.

2.4 Paradigm shift

There has been little focus on the geometric movement of the ALLS system transformation of the coordinates from one aspect of the system to another. This provides an opportunity to enhance the scan path calculations of various positions of a robot arm, scanner, and beam while scanning along a defined trajectory on a component and making the observation that point coordinates are changing continuously along that trajectory. Although a few researchers (Shen and Zhu 2012; Yin et al. 2014) have worked to determine the kinematic relation of fixed frames and moving frames like a robot and laser line scanner (Yin et al. 2014), as well as the relation between tool and the component systems with respect to a three degree of freedom machine (Kim et al. 2015), there has been little research focused on the integration of all three elements (robot, scanner, and component surface) to determine the geometric coordinate changes along a trajectory path of a component surface. This gap leads to a paradigm shift on the approach of solving the problem of obtaining better point cloud data by integrating the ALLS system and component

surface coordinate systems. The determination of such a relation provokes the need to understand the geometric transformation of coordinates during the scanning movement of the ALLS system. Thus, it is critical to determine the changing kinematic structure during the movement of the entire ALLS system while moving across a trajectory for a given component to fully understand the kinematic mechanism occurring during point cloud measurements (Buchsbaum and Freudenstein 1970).

The system's mechanical linkages move along a fixed trajectory on the surface of a component, which changes the position and orientation of coordinates of the three elements of system. This movement is fixed at the robot base, while other joints up to the laser beam move as one mechanical linkage along a trajectory. As a result, the orientation transformation matrix of the end effector, laser scanner, and laser beam joints can be obtained. The coordinates of the points on the trajectory of a component are calculated by solving the geometrical equations of the shape of the component surface, assuming the component is fixed with respect to the robot's base. However, to move all the mechanical linkages to this fixed point on the component, the joint angles of robot (θ_1, θ_6), laser line scanner (θ_{ls}), and laser beam (θ_{beam}) must be determined by using inverse kinematic equations for six degree FANUC S430 IW robot (Odeyinka and Djuric 2016). Thus, we can understand the geometrical transformation from one coordinate system transform to another coordinate while moving the system along a scan path. This helps to determine the position coordinates for the end effector, laser scanner, and beam to move on a trajectory point on the surface of the component.

2.2 Related kinematic models

Several researchers (Vincze, Prenninger et al. 1994; Leigh-Lancaster, Shirinzadeh et al. 1997; Feng, Liu et al. 2001; Santolaria, Guillomía et al. 2009; Wang, Mastrogiacomo et al. 2011;

Paoli and Razionale 2012; Norman, Schönberg et al. 2013) have targeted the kinematic relation between a robot and a laser line scanner using an external laser tracking system. The kinematic relation between the robot and laser scanner without an external tracker using a linear rail type of a moving linkage to support a stationary laser scanner (Yin et al. 2014) and the relation between three degree of freedom machine, tool, and component system with respect to an arbitrary component surface (Kim et al. 2015) are extended in this work by determining the kinematic relationship for a six degree of freedom robot, scanner, and spherical component surface during the scanning motion. The position and orientation coordinates for each element of the system determine the position and orientation of the robot end effector $O_e(x_e, y_e, z_e)$ and laser scanner $O_s(x_s, y_s, z_s)$ while the robot is in arbitrary motion, as shown in Figure 2. The geometric transform relationship between the robot end effector frame and the laser scanner without an external tracker is called the hand-eye calibration of a laser probe and robot (Dornaika and Horaud 1998; Yin et al. 2014).

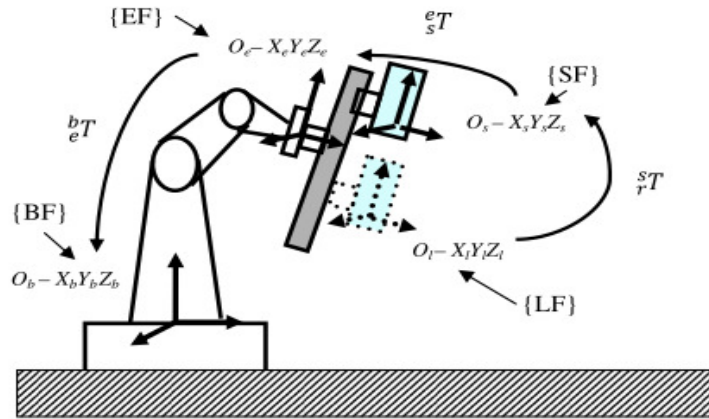


Figure 2: Integrated 3D scanning system (Yin, Ren et al. 2014)

As shown in Figure 2, a fixed scanner and sensor are mounted on a moving scanning frame as a rail frame. The end effector (EF) of robot has coordinates $O_e(x_e, y_e, z_e)$, scanning frame (SF)

$O_s(x_s, y_s, z_s)$, and linear frame (LF) has coordinates $O_l(x_l, y_l, z_l)$ with respect to the robot base coordinates $O_s(x_b, y_b, z_b)$. The shape and position information of local features within the range of the rail frame are obtained by multiplying 4x4 homogenous matrices as described in Yin et al. (2014), Eq. 1 derives the relationship between the coordinate, P_b , in the robot base frame and P_l in the laser sensor frame.

$$P_b = T_e^b * T_s^e * T_l^s * P_l \quad \text{Eq. (1)}$$

Where T_e^b , T_s^e and T_l^s are 4x4 homogenous coordinate transform matrices. T_l^s is the transform relationship between the laser sensor and the rail scanning frame, T_s^e is transformation between the rail scanning frame and robot end effector frame, T_e^b denotes transform relationship between the robot end effector and the robot base. The model in Figure 3 (Yin et al. 2014) formulates the relationship between the spheres centers measured for different robot poses with the laser sensor frame changes. These models provide insight into formulating the relationship between different coordinate frames of each element of this ALLS system.

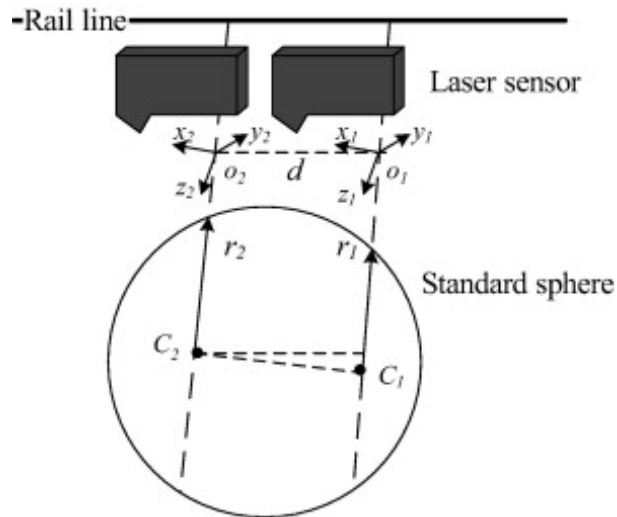


Figure 3: Relationship between the scanning frame and robot frame (Yin et al. 2014)

A similar approach establishes the kinematic relationships between the tool coordinate system with the component with respect to three-axis prismatic machines (Kim et al. 2015). In

their work as shown in Figure 4, the tool frame (x_t, y_t, z_t) is perpendicular to the arbitrary component surface (x_a, y_a, z_a) . The steps to plan the trajectory are as follows: derive the surface tangent vectors of the curved surface in the component local coordinate system, determine the forward kinematics from the local coordinate and the tool coordinate, and calculate the joint parameters using inverse kinematics. While this application is not targeted for laser line scanners, it contributes towards developing the approach for the orientation of the laser scanner perpendicular to the component in order to determine the kinematic relationship between a laser line scanner and component coordinates with respect to the robot base (x_b, y_b, z_b) .

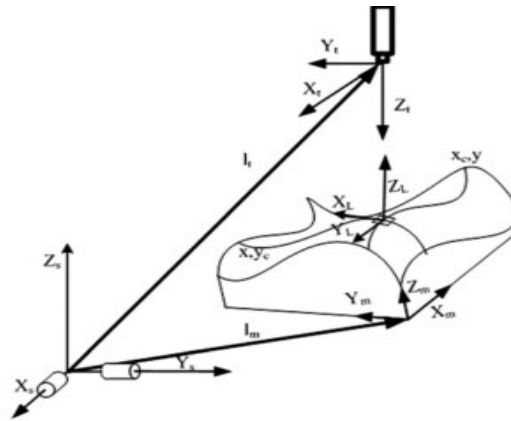


Figure 4: Kinematics of robot-base, tool, and surface for a wire embedding process (Kim et al. s 2015).

This research fills the research gap to undertake the study of geometric coordinates in automated laser scanning system elements relative to component surface. The summary of literature review is presented in the Table 1, which provides the gap of this research and helps to understand this thesis contribution. The distinguishing elements of the ALLS system in our research are the six degree of freedom robot, laser scanner, and stationary component instead of a three degree of freedom robot and tool (Kim et al. 2015), or a rail scanning frame to support the stationary laser scanner, laser sensor, and component mounted on a turntable (Yin et al. 2014).

REFERENCE RELATION	CMM/ scanner model	6DOF robot model	Six-degree of freedom robot and laser scanner	Three degree of freedom, tool, component	6DOF, scanner component
Vincze et al. 1994		X	X		
Yau and Menq 1995	X				
Pauly et al. 2004	X				
Lu and Milios 1997		X	X		
Borangiu et al. 2009		X	X		
Xi and Shu 1999	X	X	X		
Son, Park et.al. 2002	X		X		
Triebel et al. 2004		X	X		
Larsson and Kjellander 2006	X	X	X		
Bračun et al. 2006	X				
Larsson and Kjellander 2008		X	X		
Jin and Yang 2009		X	X		
Shen and Zhu 2012		X	X		
Yin et al. 2014		X	X		
Kim et al. 2015		X		X	
Arachchige et al. 2014		X			
Odeyinka and Djuric 2016		X			
This Thesis		X	X		X

Table 1: Summary of literature review: explaining gap analysis and my work

3. ELEMENTS OF ALLS SYSTEM

The ALLS system is an inspection scanning system consists of laser line scanner attached as tool frame to the six degree of freedom FANUC S-430 IW robot. During scanning motion, as this inspection system is moved, the changes in geometry of the system changes. The kinematics of the laser line scanner and the FANUC S-430 IW robot are explained in detail in this chapter.

3.1 Laser Line scanner- MetraSCAN-R scanner

Laser line scanner measurement operates by the controlled deflection and steering of laser beams, followed by a distance measurement at every pointing direction. A 3D laser scanner consists of a laser, ranging unit, and control data unit. The laser unit is a deflecting or rotating unit that produces the laser beam or pulse that is needed for measurement. The ranging unit is a signal processing unit in which distances and angles are determined. To develop an ALLS system the triangulation of 3D laser scanners must be known. A laser stripe projects onto the component surface, and the reflected beam is detected by cameras. Through this method, the three dimensional coordinates are acquired. The laser line is a function of the view angle limit, the location vector of the source, the stand-off distance, and a vector perpendicular to the laser source (Son et al. 2002). The laser projector and sensor are modeled as the coordinate systems of the laser projector, the lens, the sensor, and the component surface (Bračun et al. 2006). A scanning system automatically finds an optical focus and maintains a certain distance, called a stand-off distance, between the end of the laser probe and the beam focused on the component; refer to Figure 5 (Bračun et al. 2006). The incident beam and reflected beam should not interfere with the part itself. The laser scanner should be kept at a collision free distance from the component surface.

The certain parameters of the laser scanner required for scanning a point on a surface are defined as follows:

- **View Angle:** The angle between the incident laser beam and the surface normal of a point being measured should be less than the rotation angles. This is the orientation of the scanner relative to the component surface. This is kept perpendicular relative to the component surface.

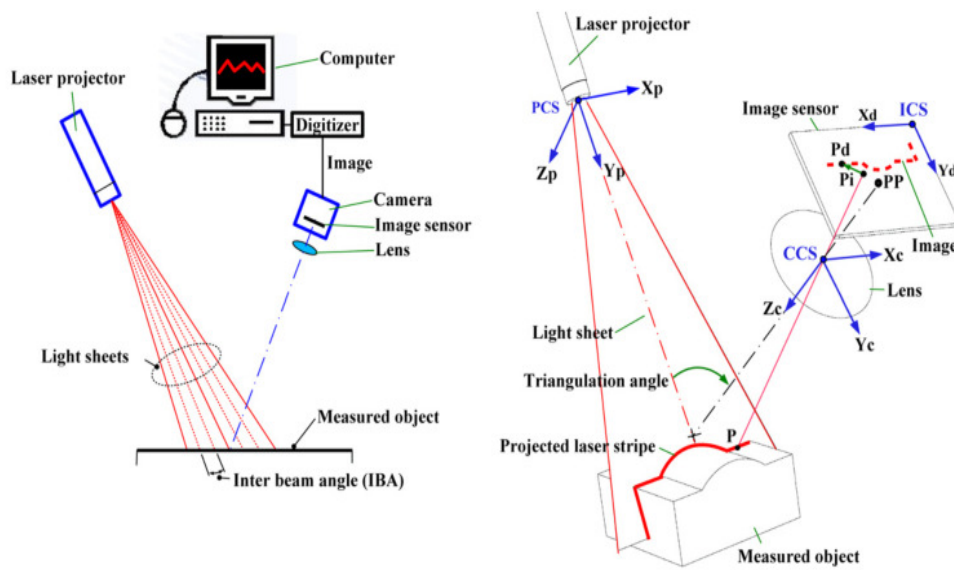


Figure 5: Laser line scanner parameters (Bračun, Jezeršek et al. 2006)

- **Field of View:** The measured point on the part surface should be within the length of the laser stripe.
- **Depth of View:** The measured point should be within a specific range of distance from the laser source.

3.2 FANUC S-430 IW Robot

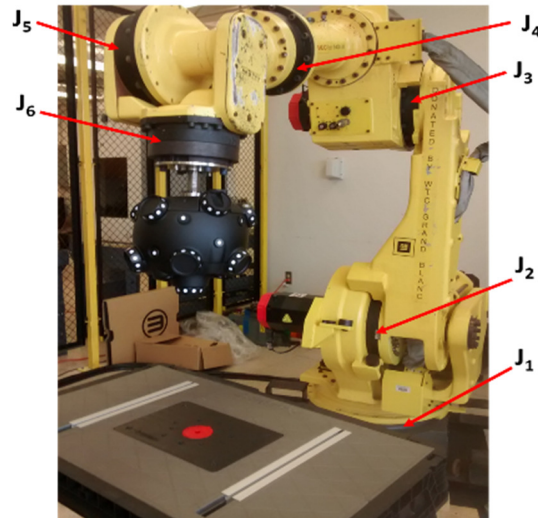


Figure 6: FANUC S430 IW robot with MetraSCAN-R 3D laser scanner attached to its end-effector

The FANUC S-430 IW robot arm, as shown in Figure 6, has six joints (J_1 , J_2 , J_3 , J_4 , J_5 , and J_6) whose kinematic relation is defined by the Denavit–Hartenberg parameters as follows: link length d_i , link offset a_i , joint angle θ_i , and twist angle α_i , where $i=1,2,3,4,5,6$ (Denavit, 1955). The MetraSCAN-R 3D laser line scanner has two intersecting laser beams. The intersection of these two laser beams defines the reference point of the laser beam coordinate frame for the presented kinematic models. The scanner is mounted on the FANUC S-430 IW, as shown in Figure 6. The tool center point of the laser scanner is defined in the tool frame to create a Z-offset that is the distance from the end of robot arm to the scanner top joint portion; see Figure 7.

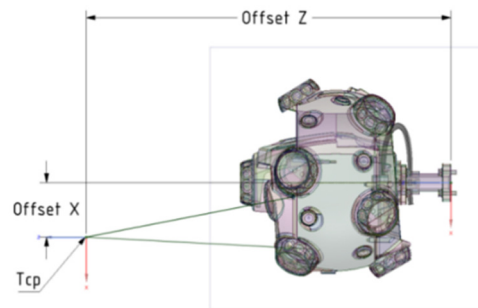


Figure 7: Offset of the Creaform MetraSCAN-R laser line scanner (MetraSCAN AutoCAD file)

3.3 The Set-Up Construction

The setup considered in this thesis consists of a six degree of freedom FANUC S-430 IW robot; its end-effector is a Creaform MetraSCAN-R 3D laser line scanner and the component surface, as shown in Figure 8. The robot end effector laser line scanner works as a kinematic mechanism to move towards the component location. The MetraSCAN-R is screwed to an interface adaptor on the robot in order to attach it to the robot. The laptop central processing unit controls the MetraSCAN-R scanner to acquire a scan image from the Vx elements software. The C-track camera is connected to the controller and the controller is connected to the laptop, as shown in below Figure 8 to complete the system setup.

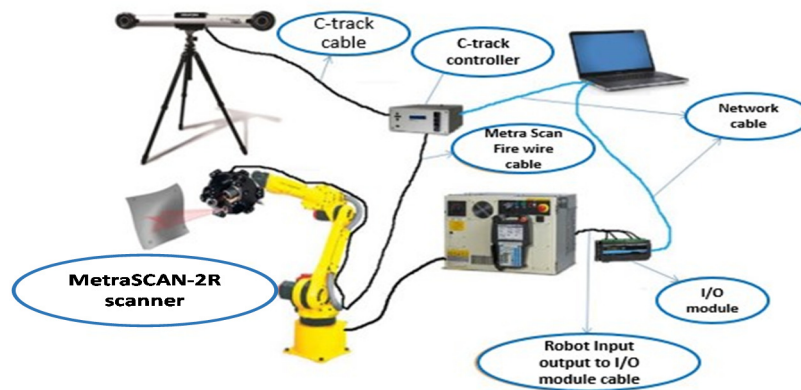


Figure 8: System components of ALLS system (MetraSCAN training script)

The C-track is calibrated initially so that the camera can view the defined scanning volume range, and different positions of the scanner. This mechanism is for registering for points located on the component by locating the scanner in the scan space. It is mandatory to perform basic training to calibrate the c-track camera, there are different scan volumes 3.08m^3 and 7m^3 depending upon the requirement, whereas for my experiment I calibrated the c-track for 3.08m^3 using Vx Elements software.

4. MODELING OF ALLS SYSTEM

The kinematics modeling is accomplished by following the below steps:

- i. Solve the forward kinematics equations for the six degree of freedom robot, the laser scanner, and the laser beam. This validates the position of the model of the entire measurement system.
- ii. Define the component surface by calculating the equation of the surface and point coordinates on its surface.
- iii. Calculate the joint angles for the robot, scanner, and beam using inverse kinematic equations and move the robot to the point on the component's surface to get a trajectory path for scanning.

4.1 Forward Kinematics, Step (i):

Mechanical linkages of the system are validated by solving forward kinematics by defining the position coordinates of the robot end effector, scanner, and beam. The validation position for the FANUC LR 200 IC robot is obtained by Arachchige et.al (2014), but it is extended in this research by solving the forward kinematic equations to obtain the validated position for the FANUC S-430 IW robot, laser scanner, and laser beam. The kinematic structure of the FANUC S-430 IW, MetraSCAN-R scanner, and beam are shown in Figure 9. The relationship between the two links of the joints can be described using Denavit and Hartenberg (1955) parameters represented as follows: link lengths (d_1-d_6) (Kashani et.al. 2010), link offset (a_1-a_6), joint angles ($\theta_1-\theta_6$), and twist angle ($\alpha_1-\alpha_6$) for the robot. The scanner is added as the tool frame, where a_{ls} is the width of laser scanner, a_{beam} is the width of the beam from its cross-section, d_{ls} is the length of the scanner, d_{beam} is the length of the laser stripe and stand-off distance, α_{ls} is the twist angle of the laser scanner, α_{beam} is the twist angle of the laser beam, θ_{ls} is the joint angle of the laser scanner,

and θ_{beam} is the joint angle of the laser beam, Table 2. It is assumed that d_{beam} , is constant. While d_{beam} is considered constant in this work, the scanner allows for a minimum and maximum stand-off distance; thus, subsequent kinematic models must account for a variable Z-offset within the allowable range. Individual homogenous transformation matrices ${}^{i-1}P_i$ for the i^{th} joint of robot are expressed as Eq. (2) of Arachchige et al. (2014), where $i=1, 2, 3, 4, 5, 6$ joints of robot. The resultant matrix, 0P_6 , is obtained by multiplying all homogenous transformation matrices; ${}^{i-1}P_i$ is expressed by Eq. (3), which is the position and orientation of the robot arm.

$${}^{i-1}P_i = \begin{bmatrix} \cos \theta_i & -\cos \alpha_i \sin \theta_i & \sin \alpha_i \sin \theta_i & a_i \cos \theta_i \\ \sin \theta_i & \cos \alpha_i \cos \theta_i & -\sin \alpha_i \cos \theta_i & a_i \sin \theta_i \\ 0 & \sin \alpha_i & \cos \alpha_i & d_i \\ 0 & 0 & 0 & 1 \end{bmatrix} \quad \text{Eq.(2)}$$

$$P_6^0 = P_1^0 * P_2^1 * P_3^2 * P_4^3 * P_5^4 * P_6^5 \quad \text{Eq.(3)}$$

JOINT	d_i	θ_i	a_i	α_i
1	740	0	305	-90
2	0	-90	1075	180
3	0	180	-250	90
4	-1275	0	0	-90
5	0	0	0	90
6	-240	180	0	180
7	$dls=393.6$	0	$als=0$	0
8	$dbeam=400$	0	$abeam=0$	0

Table 2: D-H parameters for FANUC S430 IW, MetraSCAN-R scanner, and beam (Arachchige et al. 2014)

0P_6 is the validated pose matrix of the robot arm relative to the robot base, as expressed in Eq. (4), using the Matlab. The program for the validation of robot model is described in Appendix A. The orientation of the end-effector, relative to the robot base frame, is defined with the three vectors normal, n , represented by matrix (n_x, n_y, n_z) ; sliding, s , represented by matrix (s_x, s_y, s_z) ; and approach, a , represented by matrix (a_x, a_y, a_z) .

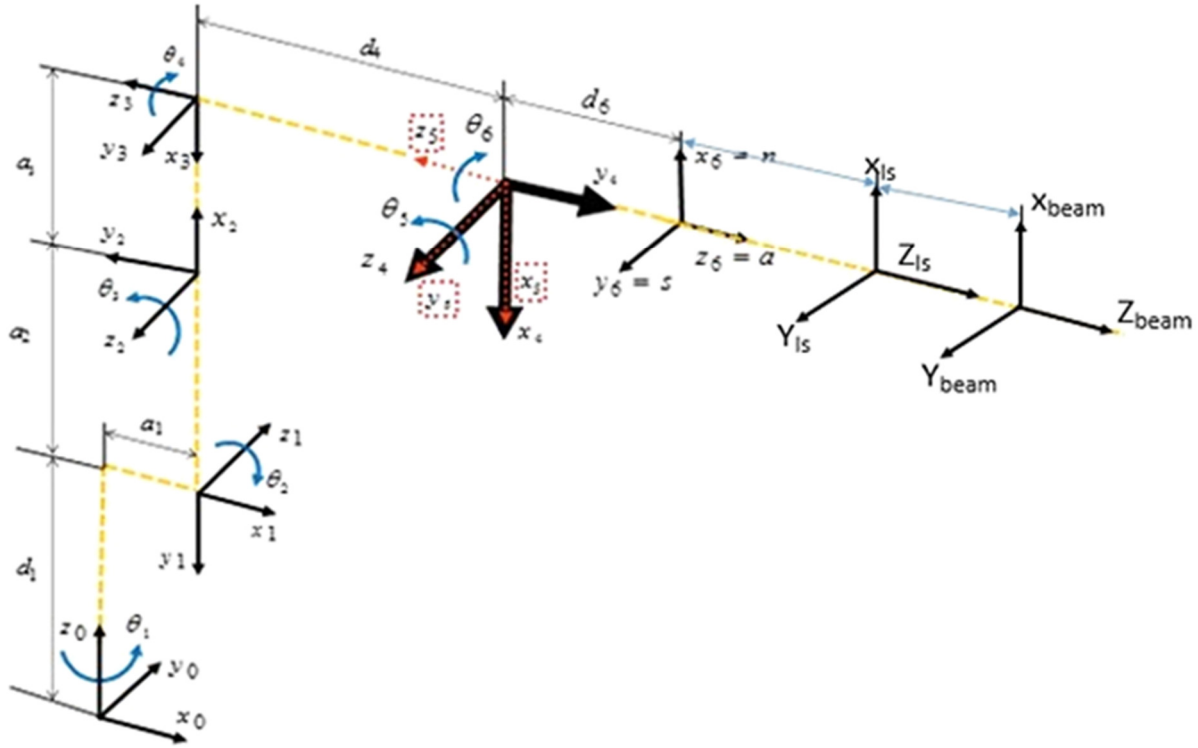


Figure 9: Kinematic model structure of measurement of point cloud system-FANUCS430 IW, Metra Scan 3D scanner and beam, addition to the Arachchige et al. (2014) model.

The last column (p_x, p_y, p_z) , represents the location and position coordinates of the validated robot arm. As per Figure 9, the end position coordinate of a validated model can be stated in kinematics as $x_6=n$, $y_6=s$ and $z_6=a$; that is, the x-coordinate is normal, the y-coordinate is sliding, and the z-coordinate approaches the vector for the end position of the model. This is similar for the scanner and beam kinematics attached to the robot (Arachchige et al. 2014).

$${}^0P_6 = \begin{bmatrix} nx & sx & ax & px \\ ny & sy & ay & py \\ nz & sz & az & pz \\ 0 & 0 & 0 & 1 \end{bmatrix} \quad \text{Eq.(4)}$$

To calculate the Denavit and Hartenberg (1955) parameters as per Figure 9 for the laser scanner $(d_{ls}, a_{ls}, \theta_{ls}, \alpha_{ls})$ and beam $(d_{beam}, a_{beam}, \theta_{beam}, \alpha_{beam})$, the actual measurements of the MetraSCAN-R are determined. These measurements on MetraSCAN-R are the link length, d_{ls} , is

the length of the tool and scanner equal to 393.6mm and the d_{beam} is the total length of the light beam and the stand-off distance is 400mm. Based on the kinematics Figure 9, the Z-axis of the scanner is parallel to the Z_6 axis of joint 6. The d_{ls} is the distance between the two X-axes, joint 6 (X_6) and scanner (X_{ls}) and d_{beam} is the distance between the scanner X_{ls} and X_{beam} . The joint and twist angles for the validation position of the scanner and beam (θ_{ls} , θ_{beam} , α_{ls} , α_{beam}) are equal to zero because these are not rotated along the Z-axis or X-axis. The offset length parameter a_{ls} is the width of the scanner, according to kinematic structure, and the distance between the two Z-axes, Z_6 and Z_{ls} , is zero; a_{ls} is zero. The beam center point Z-axis is also parallel to the Z axis of the scanner, so the a_{beam} is also equal to zero. The individual homogenous matrix for the laser scanner, P_{ls} , is represented by Eq. (5). Then, by multiplying Eqs. (4) and (5), Eq. (6) is obtained, and the resultant matrix $P_{scanner}$ is the validated position and the orientation of the laser scanner.

$$P_{ls} = \begin{bmatrix} \cos \theta_{ls} & -\cos \alpha_{ls} \sin \theta_{ls} & \sin \alpha_{ls} \sin \theta_{ls} & a_{ls} \cos \theta_{ls} \\ \sin \theta_{ls} & \cos \alpha_{ls} \cos \theta_{ls} & -\sin \alpha_{ls} \cos \theta_{ls} & a_{ls} \sin \theta_{ls} \\ 0 & \sin \alpha_{ls} & \cos \alpha_{ls} & d_{ls} \\ 0 & 0 & 0 & 1 \end{bmatrix} \quad \text{Eq.(5)}$$

$$P_{scanner} = {}^0P_6 * P_{ls} \quad \text{Eq.(6)}$$

Similarly, the individual homogenous matrix for a laser beam is expressed as Eq. (7); by multiplying Eqs. (6) and (7), the resultant matrix P_{laserb} , Eq. (8) is obtained for the validated position and orientation of the laser beam. Hence, the position coordinates of the validated model are in the last column of the first three rows of the matrix P_{laserb} (X_{laserb} Y_{laserb} Z_{laserb}).

$$P_{beam} = \begin{bmatrix} \cos \theta_{beam} & -\cos \alpha_{beam} \sin \theta_{beam} & \sin \alpha_{beam} \sin \theta_{beam} & a_{beam} \cos \theta_{beam} \\ \sin \theta_{beam} & \cos \alpha_{beam} \cos \theta_{beam} & -\sin \alpha_{beam} \cos \theta_{beam} & a_{beam} \sin \theta_{beam} \\ 0 & \sin \alpha_{beam} & \cos \alpha_{beam} & d_{beam} \\ 0 & 0 & 0 & 1 \end{bmatrix} \quad \text{Eq.(7)}$$

$$P_{laserb} = P_{beam} * P_{scanner} \quad \text{Eq.(8)}$$

4.2 Component surface, Step (ii):

The assumption of our model to transform the relationship from the laser scanner frame to the component surface frame states that the component is a sphere. The approach can be applied to other component surfaces by replacing this surface representation. More complex surfaces may require integration with CAD model data. The spherical coordinate system is used for specifying the position of the point on the surface (Fu et.al. 1987), which involves the following translations or rotations: translation of the radius, r , in the Z-axis direction; rotation, α , about the Z-axis; and rotation, β , about the x-axis. The Matlab program for deriving the equation of component surface is described in Appendix B.

4.3 Inverse Kinematics, Step (iii):

Inverse kinematics is the approach for general serial manipulators to compute joint displacements for a given pose of the end effector (Manocha & Canny, 1994). This inverse kinematics solution is required to calculate the joint angles (θ_1 to θ_6) for six degree of freedom FANUC S-430 IW (Odeyinka. 2015; Odeyinka and Djuric 2016). In this research these inverse kinematic equations are modified slightly to validate the FANUC S-430 IW robot along with the laser scanner end-effector. The modelling of the scanner and the beam has been done by adding two frames as an offset; as a result, Eq. (9) is implemented in the inverse kinematics solutions to determine the joint angles of the robot (θ_1 to θ_6). To solve this approach the first step is to find the first three joints and then the last three joints (Pieper 1968). In the calculation of the first three joint angles the first step is to locate the intersection of the last three joints axes and calculate the position of this intersection point, from the desired position vector p and pose R of the end effector. In Figure 10, the vector p is projected onto the x_0 - y_0 plane at joint 1 of FANUC S430 IW, the link

length d_{6b} is obtained by adding link length of robot d_6 , link length of scanner d_{ls} , and link length of laser beam d_{beam} , with reference to the kinematics shown in Figure 9.

$$d_{6b} = d_6 + d_{ls} + d_{beam} \quad \text{Eq. (9)}$$

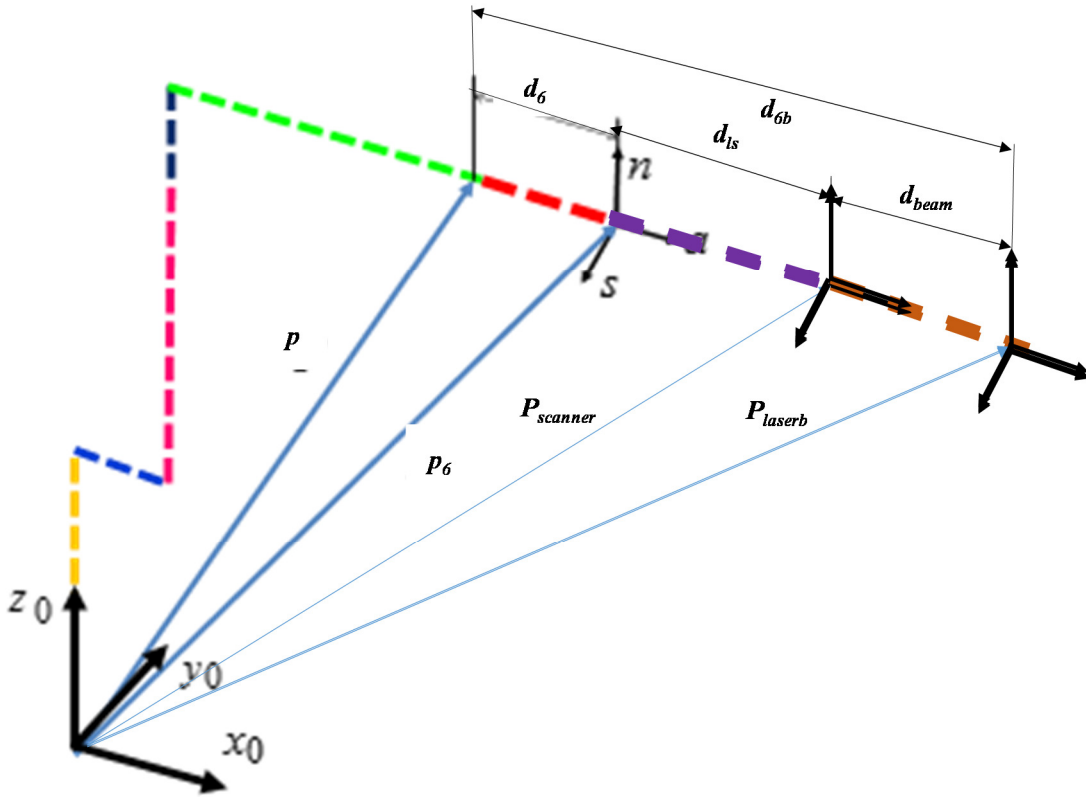


Figure 10: Position vector p for spherical wrist robots (Odeyinka, 2015).

From Eq. (9) and Figure 10, the position vector for FANUC S430 IW is calculated as:

$$p = p_6 - d_6 \cdot a = (p_x, p_y, p_z)^T \quad \text{Eq. (10)}$$

The position vector for FANUC S430 IW is calculated when the MetraSCAN-R and the beam are added as tools to the robot, then d_6 becomes d_{6b} as per the Eq.(9) and it is inserted in Eq.(10) and Eq.(11) is obtained:

$$p = p_6 - d_{6b} \cdot a = (p_x, p_y, p_z)^T \quad \text{Eq. (11)}$$

Hence, according to Eqn. (11) each coordinate of p (p_x, p_y, p_z) is calculated from Eq. (10) is mentioned in Eq. (12) as:

$$\begin{aligned} px &= p_{x6} - abs(d_{6b}) \cdot a_x \\ py &= p_{y6} - abs(d_{6b}) \cdot a_y \\ pz &= p_{z6} - abs(d_{6b}) \cdot a_z \end{aligned} \quad \text{Eq. (12)}$$

Whereas, P_{x6} , P_{y6} , and P_{z6} in Eq. (12) are the position vector of 0P_6 the values of last column of matrix and a_x , a_y , and a_z are the approach vector of P_6 , the values of third column of matrix obtained from Eq. (4).

4.3.1 Joint 1 solution:

The joint 1 solution for FANUC S-430IW is obtained by projecting the position vector p onto x_0 - y_0 . The position vector p , points from the origin of the shoulder coordinate system to the point where the last three joints axis are intersecting. The last three joint axes intersect at point D . This point is the Wrist Center Point (WCP) as shown in Figure 11. Motion of the final three joints about these axes will not change the position of D . Position of the wrist center is a function of only the first three joint angles (Odeyinka and Djuric 2016). The ARM, ELBOW and WRIST definitions for FANUC robot family are discussed (Odeyinka and Djuric 2016):

- I. Left Arm (LA): when positive θ_2 moves the wrist in negative direction while θ_3 is not active
- II. Right Arm (RA): when positive θ_2 moves wrist positive z_0 direction while θ_3 is not active.
- III. Above Arm or Elbow above wrist: when the position of the wrist to the RA/LA with respect to the shoulder coordinate system has negative/positive coordinate value along the y_2 axis.
- IV. Below Arm (BA) or Elbow Below wrist: When the position of the wrist to the RA/LA with respect to the shoulder coordinate system has positive/negative coordinate value along the y_2 axis.

angle of Joint 2. The geometric representation shows θ_1 and θ_2 in Figure 12 and in triangle BCD, length BD is calculated using Pythagoras theorem, as shown in Eq. (17) and from triangle ABD, the β angle is calculated, using the trigonometry, sine and cosine β values expressed in Eq. (18), (20). In triangle AED, r , length of AE is calculated using Eq. (19)

$$BD = \sqrt{d_4^2 + a_3^2} \quad \text{Eq. (17)}$$

$$\sin \beta = \pm \sqrt{1 - \cos^2 \beta} \quad \text{Eq. (18)}$$

$$r = \sqrt{px^2 + py^2} \pm a_1 \quad \text{Eq. (19)}$$

$$\cos \beta = (a_2^2 + R^2 - a_3^2 - d_4^2) / (2 * R * a_2) \quad \text{Eq. (20)}$$

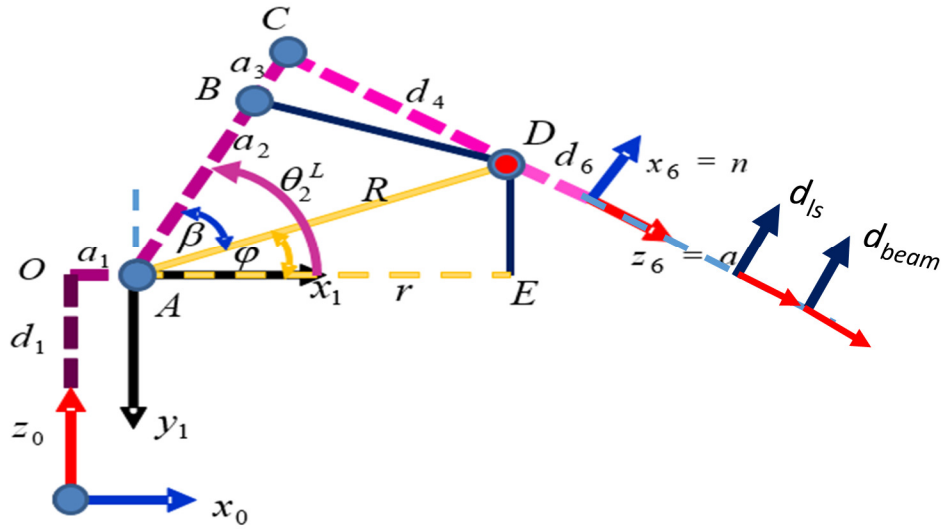


Figure 12: Projection of vector P onto $x_1 - y_1$ for Joint 2 (Odeyinka and Djuric 2016)

Here, Eq. (18) is always positive and AE is the distance r , $+a_1$ is for LEFT ARM and $-a_1$ is for RIGHT ARM in Eq. (14). The distance R is calculated from Eq. (21)

$$R = \sqrt{(\sqrt{px^2 + py^2} - a_1)^2 + (pz - abs(d_1))^2} \quad \text{Eq. (21)}$$

From Triangle AED of Figure 12, the distance DE is given by Eq. (22) and sine, cosine values of ϕ is given by Eq. (23) and (24). To calculate θ_2 is the inverse tan ratio, using trigonometry is obtained by Eq. (27) by calculating the sine, cosine values of θ_2 is given by Eq. (25) and (26)

$$DE = p_z - d_1 \quad \text{Eq. (22)}$$

$$\sin \phi = \frac{(p_z - abs(d_1))}{R} \quad \text{Eq. (23)}$$

$$\cos \phi = \frac{-r}{R} \cdot ARM \quad \text{Eq. (24)}$$

$$\sin \theta_2 = \sin \phi * \cos \beta + ARM \cdot ELBOW \cdot \cos \phi \cdot \sin \beta \quad \text{Eq. (25)}$$

$$\cos \theta_2 = \cos \phi * \cos \beta + ARM \cdot ELBOW \cdot \sin \phi \cdot \sin \beta \quad \text{Eq. (26)}$$

$$\theta_2 = \tan^{-1} \frac{\sin \theta_2}{\cos \theta_2} \quad \text{Eq. (27)}$$

Further the ELBOW configuration is defined as the position of the wrist with respect to the shoulder coordinate system, which has negative or positive coordinate value along the y_2 -axis, and this is the Above Arm or Elbow Above wrist. The position of the wrist to the RIGHT/LEFT Arm with respect to the shoulder coordinate system has a positive or negative coordinate value along y_2 axis. The decision equation is defined by 2P_4 in Eq. (28) and the ARM indicator from Eq. (14). The sign of the decision equation for the ELBOW indicator Eq. (28) is based on the sign of y -component of the position vector of 3P_2 , 4P_3 , and ARM indicator. There are different values for joint 3 as shown in Table 3.

$${}^2_4P = {}^3_2P \cdot {}^4_3P$$

$${}^2_4y = P_4(1, 2) \quad \text{Eq. (28)}$$

$$ELBOW = ARM * sign({}^2_4y)$$

4.3.2 Joint 3 solution:

Consider projection of position vector p onto plane x_2 - y_2 solution.

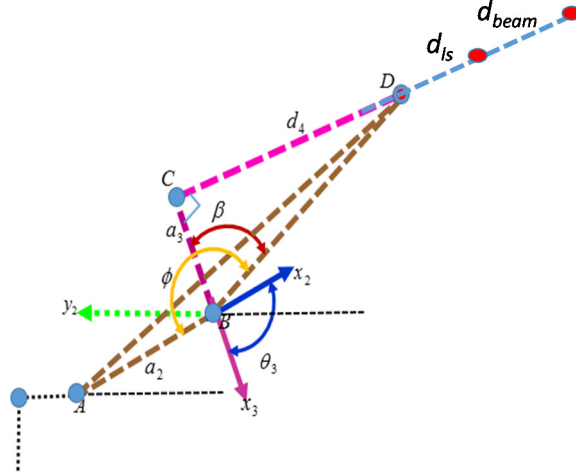


Figure 13: Projection of vector P onto x_2 - y_2 for Joint 3 (Odeyinka and Djuric 2016)

From the geometry of Figure 13, it is given that $AB = a_2$, $BC = a_3$ and $CD = d_4$

therefore Eq. (29) is obtained,

$$\theta_3 = 360 - (\phi - \beta) \quad \text{Eq. (29)}$$

From triangle BCD applying trigonometry, sine and cosine values of ϕ by Eq. (30) & (31) are obtained as:

$$\cos \phi = \frac{a_2^2 + a_3^2 + d_4^2 - (AD)^2}{2 * a_2 * \sqrt{a_3^2 + d_4^2}} \quad \text{Eq. (30)}$$

$$\sin \phi = \sqrt{1 - \cos^2 \phi} \quad \text{Eq. (31)}$$

From Triangle BCD, sine and cosine values of β from Eq. (32) & (33) are as:

$$\cos \beta = \frac{abs(a_3)}{\sqrt{a_3^2 + d_4^2}} \quad \text{Eq. (32)}$$

$$\sin \beta = \frac{abs(d_4)}{\sqrt{a_3^2 + d_4^2}} \quad \text{Eq. (33)}$$

The sine and cosine values of θ_3 are given by Eq. (34) & (35) by inserting Eq. (30) – (33)

$$\sin \theta_3 = \cos \phi * \sin \beta - \sin \phi \cos \beta \quad \text{Eq. (34)}$$

$$\cos \theta_3 = \cos \phi * \cos \beta + \sin \phi \cdot \sin \beta \quad \text{Eq. (35)}$$

$$\theta_3 = \tan^{-1} \frac{\sin \theta_3}{\cos \theta_3} \quad \text{Eq. (36)}$$

Arm Configuration	$({}^2P_4)_y$	θ_3	ARM	ELBOW	ARM ELBOW
LEFT and ABOVE	≥ 0	$\alpha - \beta$	-1	+1	-1
LEFT and BELOW	≤ 0	$\alpha - \beta$	-1	-1	+1
RIGHT and ABOVE	≤ 0	$\alpha - \beta$	+1	+1	+1
RIGHT and ABOVE	≥ 0	$\alpha - \beta$	+1	-1	-1

Table 3: Different possible arm configurations for joint three (Odeyinka and Djuric 2016)

4.3.4 Joint 4 Solution:

To determine the joint angle θ_4 solution, we have to find H , which is the transformation matrix obtained, Eq. (37), is by multiplication of first three matrices with respect to the base frame

$$H = {}^0_3P = {}^3_2P * {}^2_1P * {}^1_0P \quad \text{Eq. (37)}$$

$$H = \begin{bmatrix} X_i & Y_i & Z_i & F_i \\ 0 & 0 & 0 & 1 \end{bmatrix}$$

Hence, each matrix X_3 , Y_3 , Z_3 and F_3 can be defined as:

$$X_3 = \begin{bmatrix} H(1,1) \\ H(2,1) \\ H(3,1) \end{bmatrix} \quad Y_3 = \begin{bmatrix} H(1,2) \\ H(2,2) \\ H(3,2) \end{bmatrix} \quad Z_3 = \begin{bmatrix} H(1,3) \\ H(2,3) \\ H(3,3) \end{bmatrix} \quad F_3 = \begin{bmatrix} H(1,4) \\ H(2,4) \\ H(3,4) \end{bmatrix} \quad \text{Eq. (38)}$$

The joint angle θ_4 is set such that a rotation about joint five will align the coordinate system of joint six with approach vector a . Project (X_4, Y_4, Z_4) the coordinate frame on the x_3 - y_3 plane as shown in Figure 14.

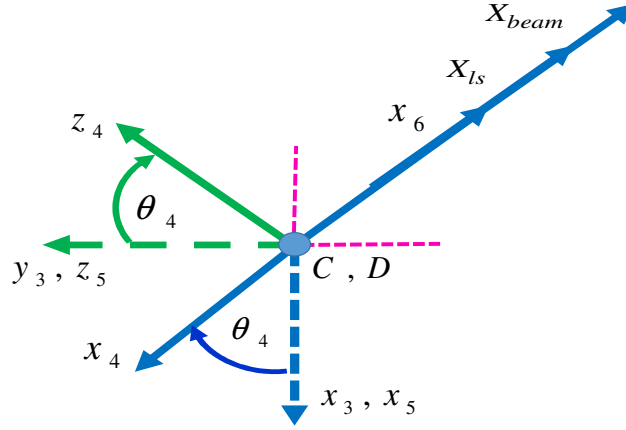


Figure 14: Rotation about joint five (Odeyinka and Djuric 2016)

In Figure 14, angle θ_4 is geometrically represented, in the positive joint direction. The detailed calculation for joint four, an angular displacement of Z_3 by rotating along approach vector Z_4 resultant matrix is obtained, Eq. (40). The transpose the matrix for approach vector, a is given by Eq. (39) as:

$$a = \begin{bmatrix} a_x \\ a_y \\ a_z \end{bmatrix} \quad \text{Eq. (39)}$$

$$Z_4 = Z_3 * a \quad \text{Eq. (40)}$$

We have Z_4, X_3 from Eqn. (38) - (40), that are used to calculate the sine and cosine values of θ_4 expressed in Eq. (41) and (42) and value of θ_4 is calculated as inverse tan ratio, using trigonometry and is expressed as Eq. (43)

$$\sin \theta_4 = -(Z_4 \cdot X_3) \quad \text{Eq. (41)}$$

$$\cos \theta_4 = -(Z_4 \cdot Y_3) \quad \text{Eq. (42)}$$

$$\theta_4 = \left(\tan^{-1} \frac{\sin \theta_4}{\cos \theta_4} \right) * \frac{180^\circ}{\pi} \quad \text{Eq. (43)}$$

There are following four solution cases of joint angle θ_4 , if the degenerate case occurs, any convenient value may be used for θ_4 as long as the orientation of the wrist (UP/DOWN) is satisfied (Lee and Ziegler, 1984)

$$\theta_4 = \left(\left(\tan^{-1} \frac{\sin \theta_4}{\cos \theta_4} \right) * \frac{180^\circ}{\pi} \right) - 90^\circ$$

$$\theta_4 = \theta_4 + \pi \quad \text{Eq. (44)}$$

$$\theta_4 = 90 - \left(\left(\tan^{-1} \frac{\sin \theta_4}{\cos \theta_4} \right) * \frac{180^\circ}{\pi} \right)$$

$$\theta_4 = \theta_4 - 180^\circ$$

The WRIST and Orientation of robot is defined by Eq. (46) - (47), Eq. (45) is assumed

$$Z_5 = -a$$

$$Y_5 = Z_4 \quad \text{Eq. (45)}$$

$$S = -Y_5$$

Hence,

$$\text{WRIST} = \text{sign}(S \cdot Z_4) \quad \text{Eq. (46)}$$

$$\text{Orientation} = \Omega = S \cdot Z_5 \quad \text{Eq. (47)}$$

4.3.5 Joint 5 solution:

To determine the joint five angle solution, the coordinate system of joint six aligns with the approach vector. As shown in Figure 15, the coordinate frame is projected on the plane x_4 - y_4 .

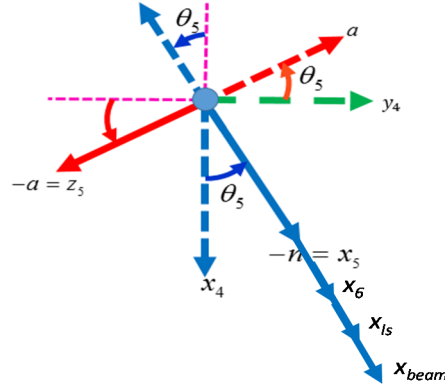


Figure 15: Rotation about joint five for joint 4 (Odeyinka and Djuric 2016)

In Figure 15, the θ_5 angle is geometrically represented using positive joint direction. The joint 5 angle, θ_5 was calculated by multiplying four homogenous matrices for joint 1,2,3,4 represented as 1P_0 , 2P_1 , 3P_2 , 4P_3 , which gives the resultant matrix, q_1 shown in Eq. (48). The elements of the matrix are stated in Table 4. Each column of the resultant matrix is represented as *n-normal*, *s-sliding*, and *a-approach*. From these X_4 , Y_4 , and a are calculated as shown in Table 4.

$$q_1 = {}^4_3P * {}^3_2P * {}^2_1P * {}^1_0P \quad \text{Eq. (48)}$$

Normal – n for q1 matrix	Sliding – s for q1 matrix	Approach – a for q1 matrix
$n_x = q_1(1,1)$	$s_x = q_1(1,2)$	$a_x = q_1(1,3)$
$n_y = q_1(2,1)$	$s_y = q_1(2,2)$	$a_y = q_1(2,3)$
$n_z = q_1(3,1)$	$s_z = q_1(3,2)$	$a_z = q_1(3,3)$
$n = n_x \quad n_y \quad n_z$	$s = s_x \quad s_y \quad s_z$	$a = a_x \quad a_y \quad a_z$
$X_4 = \text{transpose}(n)$	$Y_4 = \text{transpose}(s)$	$a = \text{transpose}(a)$

Table 4: Elements or column of Resultant Matrix q_1

The sine and cosine values of θ_5 are calculated from Eq. (49) and (50). The dot product of approach vector and X_4 gives Eq. (49) and the dot product of approach vector and Y_4 gives Eq. (49).

$$\sin \theta_5 = -(a \cdot X_4) \quad \text{Eq. (49)}$$

$$\cos \theta_5 = -(a \cdot Y_4) \quad \text{Eq. (50)}$$

For the joint 5 solution θ_5 , is obtained from Eq. (51) by inverse tan ratio of Eq. (49) and (50). If joint angle 5 obtained is $\theta_5 = 0$, then robot manipulator is said to be at singularity and cannot be moved unless and until the θ_5 is changed. The flip/no-flip configuration can be identified by the sign of θ_5 . When θ_5 is positive, it is in the flip configuration and when θ_5 is negative, it is in the no-flip configuration. All these configurations of joint 5 solutions as mentioned in Eq. (51)

$$\theta_5 = 180^\circ - \left(\tan^{-1} \frac{\sin \theta_5}{\cos \theta_5} \right) * \frac{180^\circ}{\pi}$$

$$\theta_5 = -\theta_5$$

$$\theta_5 = \theta_5 + 270^\circ$$

$$\theta_5 = \theta_5 - 270^\circ$$

Eq. (51)

4.3.6 Joint 6 solution:

To determine the joint six angle θ_6 is set to align the given orientation vector (sliding vector or y_6) and normal vector. In Figure 16, joint angle θ_6 is geometrically represented, by using positive joint direction, and the hand coordinate frame (n, s, a) is projected on the plane x_5 - y_5 .

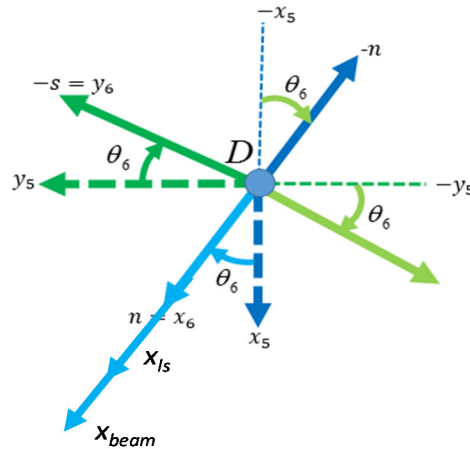


Figure 16: Rotation about joint five for joint six (Odeyinka & Djuric, 2016)

The five homogenous matrices for joint 1, 2, 3, 4, 5 represented as ${}^1P_0, {}^2P_1, {}^3P_2, {}^4P_3, {}^5P_4$ are multiplied and the q_2 resultant matrix is obtained by Eq. (52). The columns of matrix q_2 are

shown in Table 5. Using trigonometry principle, the sine and cosine values of θ_6 are calculated by Eq. (53) and (54). The joint six of robot angle θ_6 is obtained by Eq. (55) and (56)

$$q_2 = {}^5P_4 * {}^4P_3 * {}^3P_2 * {}^2P_1 * {}^1P_0 \quad \text{Eq. (52)}$$

Normal – n for q_2 matrix	Sliding – s for q_2 matrix
$n_x = q_2(1,1)$	$s_x = q_2(1,2)$
$n_y = q_2(2,1)$	$s_y = q_2(2,2)$
$n_z = q_2(3,1)$	$s_z = q_2(3,2)$
$n = \begin{matrix} n_x & n_y & n_z \end{matrix}$	$s = \begin{matrix} s_x & s_y & s_z \end{matrix}$
$X_5 = \text{transpose}(n)$	$Y_5 = \text{transpose}(s)$

Table 5: Elements of Resultant Matrix q_2

$$\sin \theta_6 = n \cdot Y_5 \quad \text{Eq. (53)}$$

$$\cos \theta_6 = s \cdot -Y_5 \quad \text{Eq. (54)}$$

$$\theta_6 = \left(\tan^{-1} \frac{\sin \theta_6}{\cos \theta_6} \right) * \frac{180}{\pi} \quad \text{Eq. (55)}$$

$$\theta_6 = \theta_6 + \pi \quad \text{Eq. (56)}$$

If degenerate case occurs according to Lee et.al, (1983), then $(\theta_4 + \theta_6)$ equals the total angle required to align the sliding vector (s) and the normal vector (n). If the flip toggle is on (i.e. FLIP=1), then Eq. (44), (51) and (56) exist. These inverse kinematics equations from Eq. (9) to (56) are validated and joint angles of robot obtained from Eq. (16), (27), (36), (44), (51) and (56) using Matlab. The Matlab program is described in Appendix C.

5. VALIDATION RESULTS FOR THE ALLS SYSTEM

5.1 Validation of Forward Kinematics for ALLS System

5.1.1 Fanuc robot S 430IW

The robot kinematics model is validated by calculation of position and orientation of selected points in 3D space and comparison of the same points using the robot teach pendant (Arachchige et al., 2014). As described in the Modelling chapter 4, the resultant matrix, Eq. (4) is obtained as a position and orientation matrix P_6^0 . A position of P_6^0 (1820, 0, 2065) mm indicates that the robot model is at the home position and is verified by using a physical robot (1820, 0, 1325) mm. The d_i is subtracted in the physical robot, for modelling purposes $d_i=740$ (Arachchige et al. (2014)). The orientation of the arm, relative to the robot base frame, is determined by three vectors: normal- n [0 0 1], sliding- s [0 -1 0] and approach- a [-1 0 0]. The validated value of $X_6 = 1820$, referred to in Figure 15, is critical in inverse kinematics equations to determine the joint angles to move the robot along a trajectory in relation to the component surface. This P_6^0 transformation matrix is validated as shown in Eq. (57), and this is the result of the validated position of the FANUC robot S-430 IW, in millimeter, plotted in Figure 17

$$P_6^0 = \begin{bmatrix} 0 & 0 & 1 & 1820 \\ 0 & -1 & 0 & 0 \\ 1 & 0 & 0 & 2065 \\ 0 & 0 & 0 & 1 \end{bmatrix} \quad \text{Eq. (57)}$$

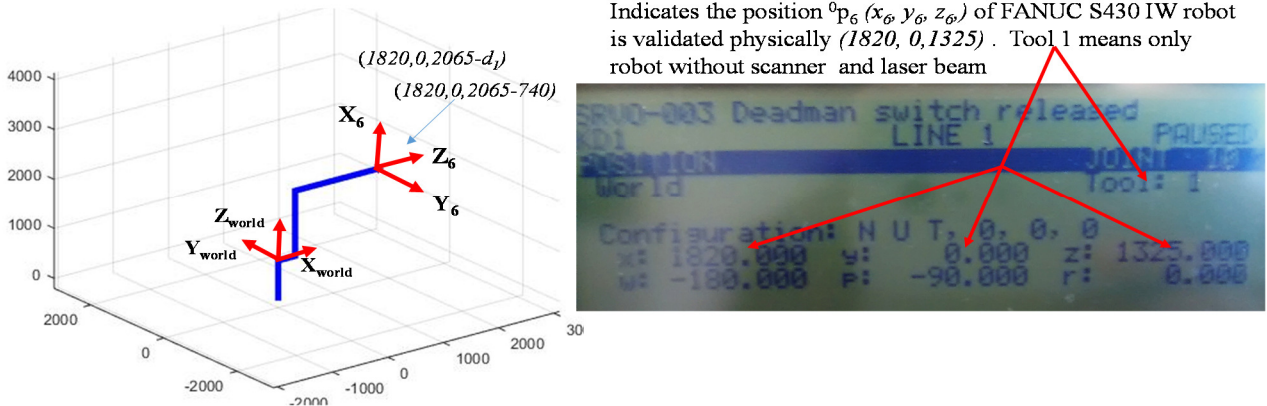


Figure 17: Validation of FANUC Robot S-430 IW model

5.1.2 Validation of the point cloud measurement system

The result of Eq. (6) is obtained as the resultant transformation matrix $P_{scanner}$ expressed in Eq. (58). The position coordinates resulting from the model are $(2213.6, 0, 2065)$ mm, which indicates that the robot end effector (*i.e.* laser line scanner) model is in its home position and orientation relative to the robot base frame, by three vectors: normal- $n [0 \ 0 \ 1]$, sliding- $s [0 \ -1 \ 0]$ and approach- $a [1 \ 0 \ 0]$, thus validating the system model. It is observed in the position coordinates that the x-coordinate increases and the z-coordinate remains constant in Eqs. (57-59). This is because the X-axis for each joint tool is parallel, and the distance between the X-axis increases along the Z-axis for each joint and the attached scanner. Since the scanner is attached to the robot and the robot and scanner must move together as one mechanical linkage, the coordinate along the Z-axis, $X_{ls} = 2213.6 \text{ mm}$, is critical to inverse kinematic equations. To calculate joint angles, the distance from X_6 to X_{ls} , (Figure 9) is d_{ls} added to d_6 in the inverse kinematic equations. Thus, joint angles are required to move the robot-scanner mechanical linkage along a trajectory.

$$P_{scanner} = \begin{bmatrix} 0 & 0 & 1 & 2213.6 \\ 0 & -1 & 0 & 0 \\ 1 & 0 & 0 & 2065 \\ 0 & 0 & 0 & 1 \end{bmatrix} \quad \text{Eq. (58)}$$

$$P_{laserb} = \begin{bmatrix} 0 & 0 & 1 & 2613 \\ 0 & -1 & 0 & 0 \\ 1 & 0 & 0 & 2065 \\ 0 & 0 & 0 & 1 \end{bmatrix} \quad \text{Eq. (59)}$$

P_{laserb} is the resultant homogenous transformation matrix, Eq. (59), representing the validation position of all the elements, the FANUC S-430 IW robot, the MetraSCAN-R laser scanner, and the laser beam. The position coordinate of the model is $P_{laserb} (2613, 0, 2065)mm$, which indicates that it is at its home position and orientation relative to the robot base frame by three vectors: normal- $n [0 \ 0 \ 1]$, sliding- $s [0 \ -1 \ 0]$ and approach- $a [1 \ 0 \ 0]$. The position and orientation of the MetraSCAN-R laser scanner and laser beam using FANUC S-430 IW is validated as shown in Figures 18 and 19, which is an extension to the existing research in Arachchige et al. (2014) for FANUC LR Mate 200IC robot. Further, the beam length is also considered as a part of the entire model. The coordinate along the Z-axis is $X_{beam} = 2613 \text{ mm}$ is also critical in calculating joint angles, where the distance from X_{ls} to X_{beam} , Figure 9, is d_{beam} and is added to the d_6 and d_{ls} value in the inverse kinematic equations to move the elements of system on the trajectory path of the component surface.

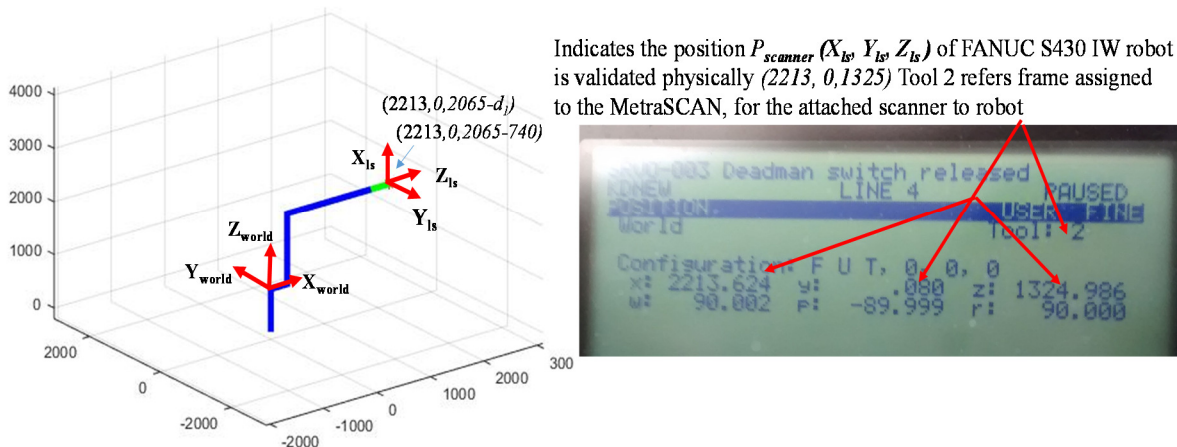


Figure 18: Validation result of the laser scanner and robot model

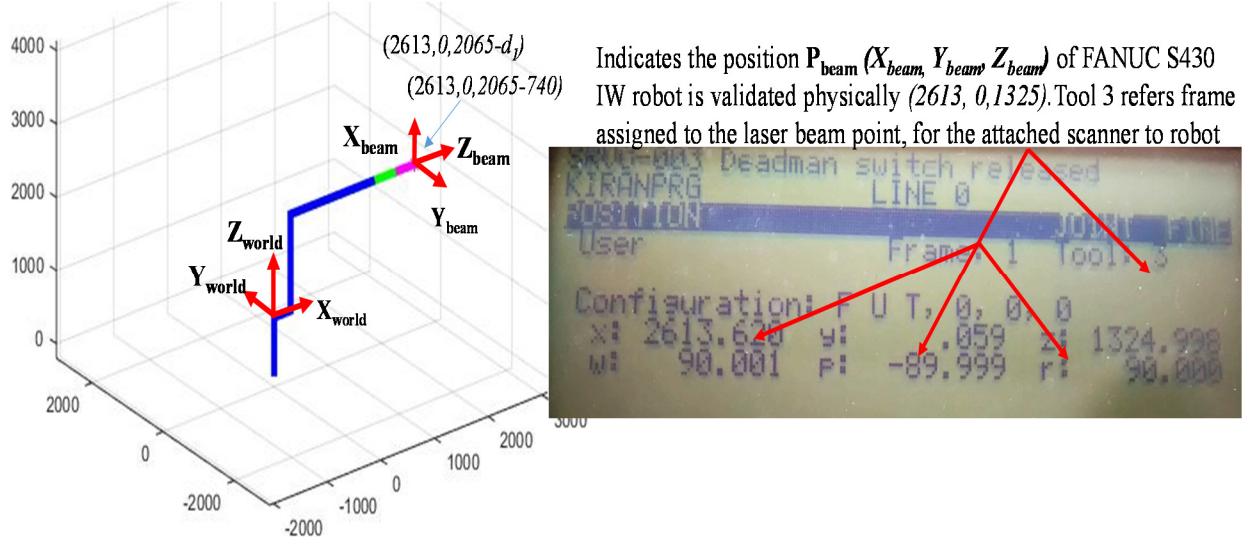


Figure 19: Validation result of the measurement point cloud system

5.2 Spherical component Surface

P_{wp} is a point obtained on the spherical surface, with radius r , expressed in homogenous transformation matrix, describing the position and orientation of this point, given by Eq. (60). Here the rotation angles α and β ranges from 0 to 180 degrees, for each of these rotation angle each corresponding point is obtained, by inserting in the below equation in Matlab, series of this points indicates a Spherical surface. The matrix and the component are plotted using the coordinates at a point P on the component as shown in Figure 20. This plotted surface acts as the trajectory path for the mechanical linkages of the system model.

$$P_{wp} = \begin{bmatrix} 1 & 0 & 0 & r * \cos\alpha * \sin\beta \\ 0 & 1 & 0 & r * \sin\alpha * \sin\beta \\ 0 & 0 & 1 & r * \cos\beta \end{bmatrix} \quad \text{Eq. (60)}$$

Hence, the position coordinates of point P_{wp} (P_{xwp} , P_{ywp} , P_{zwp}) of the spherical component is given by Eq. (61) as,

$$\begin{aligned} P_{XWP} &= r * \cos \alpha * \sin \beta, \\ P_{YWP} &= r * \sin \alpha * \sin \beta \\ P_{ZWP} &= r * \cos \beta \end{aligned} \quad \text{Eq.(61)}$$

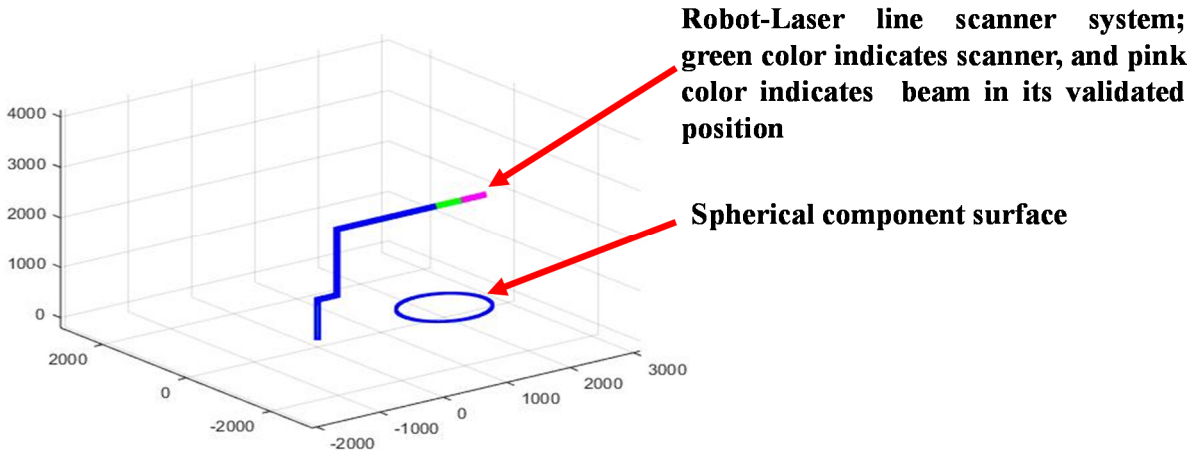


Figure 20: Validation result shows plotted equation of spherical component surface

5.3 ALLS System relative to component

When all the joint angles, except when joint 5 angle θ_5 is -90 degrees, are zero, the Fanuc robot S-430 IW is said to be in the normal relative position to the component surface, as shown in Figure 21. MetraSCAN-R scanner and its beam are added as a tool frames on the FANUC S-430 IW robot. This position of the robot is normal to the component surface required for scanning, determines the view angle of scanner. In this position the MetraSCAN-R is controlled by programming the robot and is done by Teach Pendant. The model is created using Workspace LT simulation software to demonstrate the movement of this system. Figure 22 depicts the approach of the measurement system model.

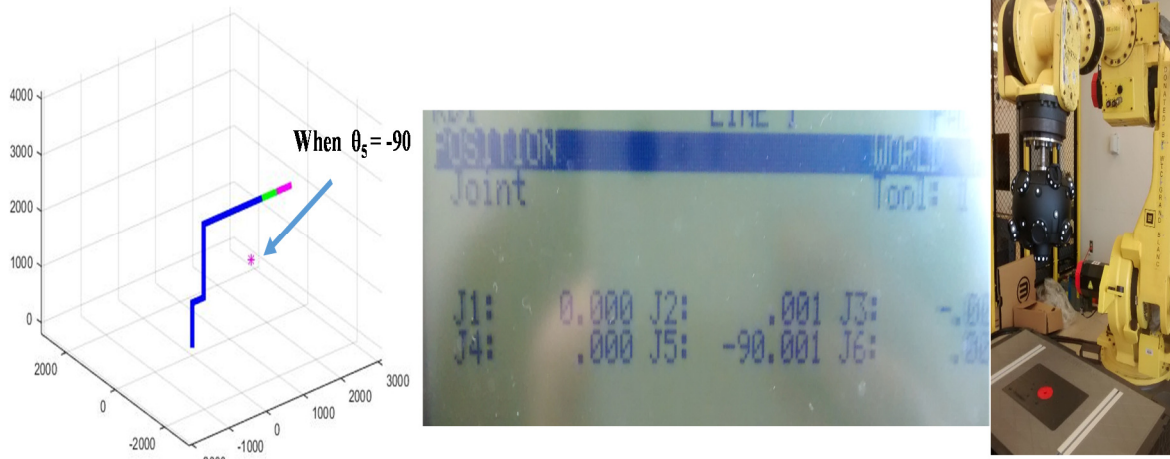


Figure 21: Inverse Kinematics validation at $\theta_1, \theta_2, \theta_3, \theta_4, \theta_6 = 0; \theta_5 = -90$

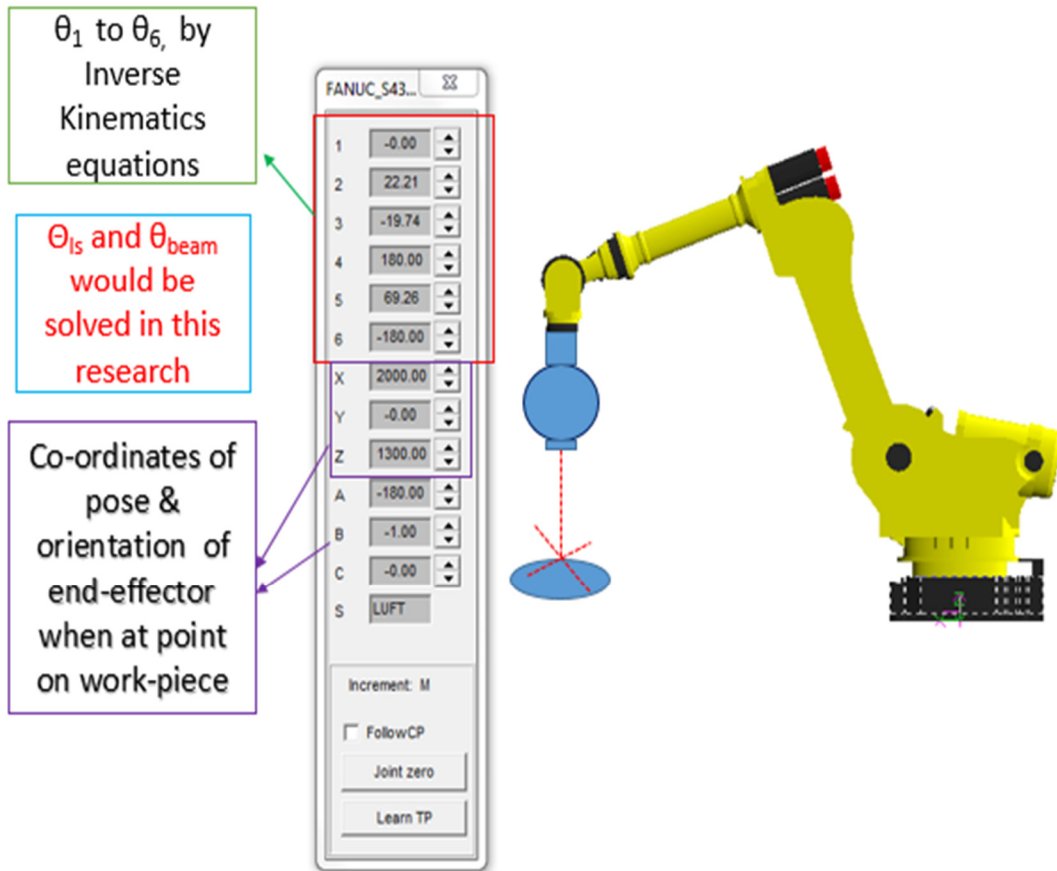


Figure 22: System movement position on the point of trajectory of component surface extension

6. SCAN PATH EXPERIMENT & RESULTS

The forward and inverse kinematic equations are validated using FANUC S430 IW robot and MetraSCAN-R system. As shown in Figure 17-19, where the resultant matrix was compared with the teach pendant actual robot position, similarly, the ALLS system moving to the component surface is validated along a particular trajectory path. The component surface is the spherical scanner calibration plate the FANUC S-430 IW robot is moved to the point on the surface; consequently the robot position is recorded. For this recorded position, the joint angles θ_1 , θ_2 , θ_3 , θ_4 , θ_5 , θ_6 are calculated to reach that measured point on the component surface. Each measured point gives a certain position of the ALLS system and the joint angle values, which establish the relation between the ALLS and the spherical component, and series of measured points gives a trajectory path. To perform the experiment for scanning a trajectory path, following steps are described: calibrating the robot, incorporating the safety limit on robot, setting a tool frame on FANUC S430 IW, calibrating the C-track, MetraSCAN-R scanner, and movement of ALLS system along a trajectory path.

6.1 Calibration of FANUC S-430 IW robot

The calibration of FANUC S-430 IW robot is usually required if the robot batteries needs to be replaced or robot loses the power. The calibration steps are shown in the FANUC calibration manual (FANUC America corporation Quick reference document). Using this manual we performed the calibration using the Teach Pendant for FANUC S-430 IW described in Figures 23, 24, 25, and 26.

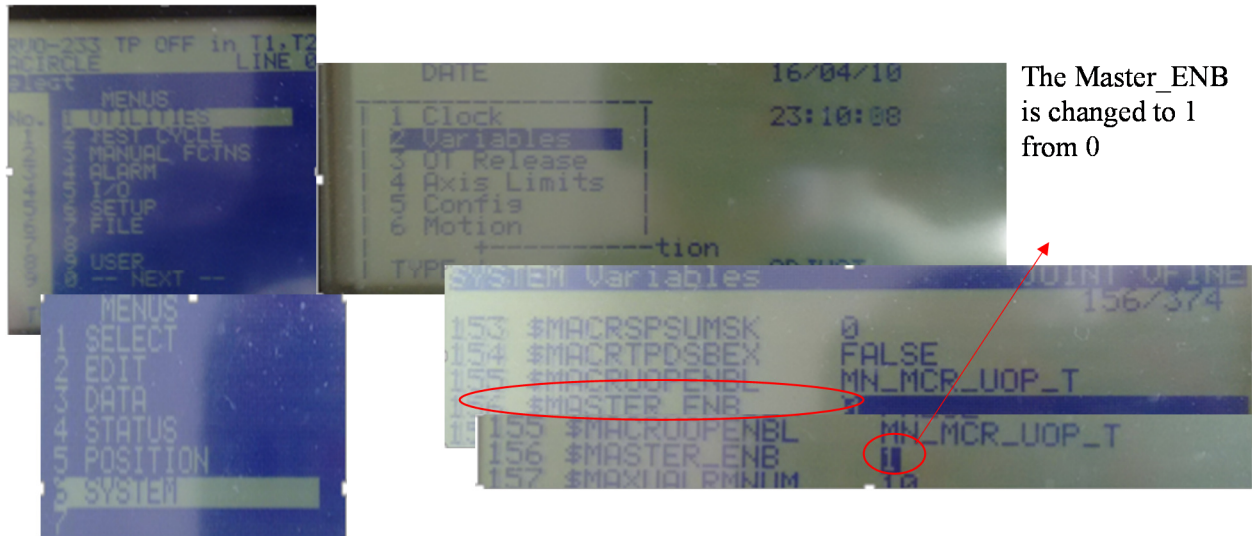


Figure 23: Master-calibration step on Teach Pendant of FANUC S-430 IW robot

On the Teach Pendant after following these steps: Press *Menu* → *select system* → Press *F1* → *select Master/ Cal*, the *Master/Cal* option screen appears, as shown in Figure 23. If the *Master/cal* is not seen on the Teach Pendant, then Press *F1* → *Variables* → *\$Master_ENB* → *set to "1" if it is "0" and press ENTER on Teach Pendant*. Go to *Master/cal* → *select the Single Axis Master-* → *check the column [ST] whether it is "0"*, → *if "0" change it to "2" for each robot axis by moving the up/down key through (MSTR_POS) column* → *Press Enter*.

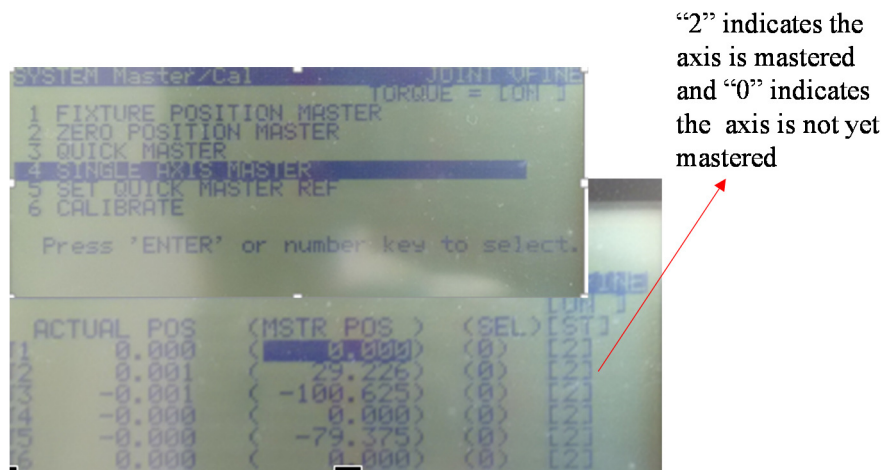


Figure 24: Single Axis Master on Teach Pendant of FANUC S-430 IW robot

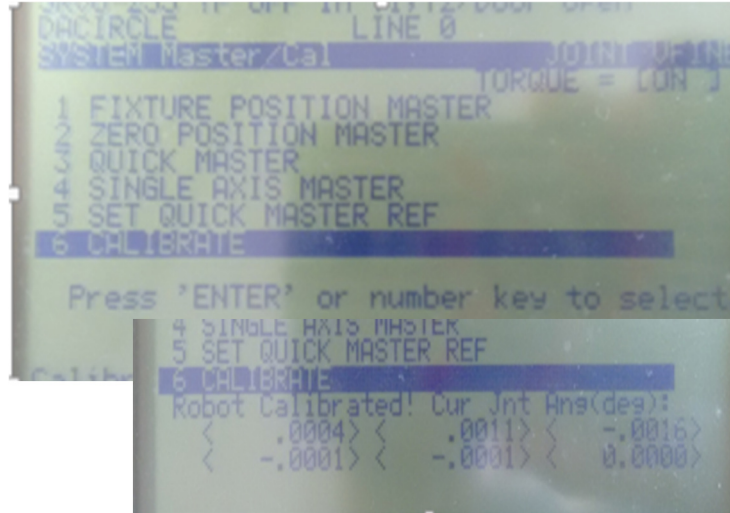


Figure 25: Calibrate on Teach Pendant of FANUC S-430 IW robot

In Master/Cal option move the cursor to 6 Calibrate position → press Enter → Press F4 it says Robot is calibrated as shown in Figure 25. Once it is done press F5. The next step mentioned in the FANUC America quick reference document is to perform single axis mastering that is for S series of robot, using the joint co-ordinate system, jog the unmastered axis of robot (J_1 - J_6) to align it with a zero degree witness mark, as shown in Figure 26.

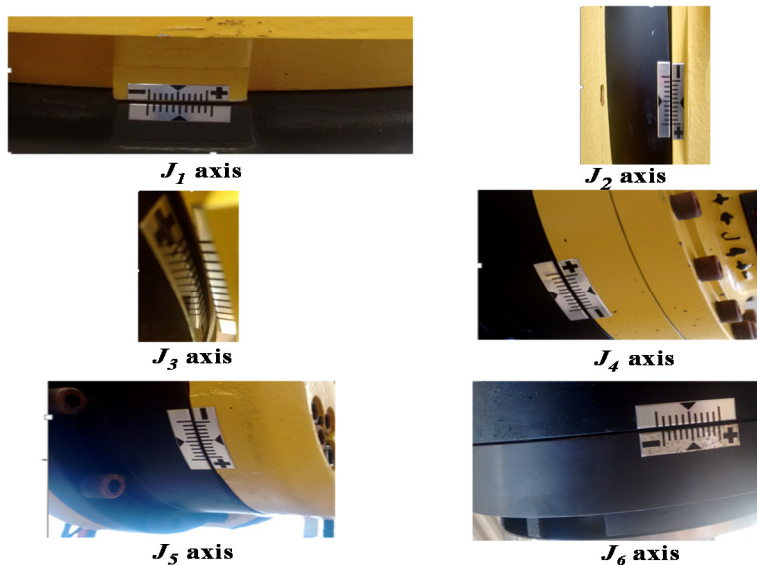


Figure 26: Jogging the unmastered Axis of all Joints J_1 to J_6 axis of FANUC S-430 IW robot using Teach Pendant

6.2 Safety limit on FANUC S430 IW robot

Before the scanning experiment was performed, it was necessary to activate the safety limits to protect the laser line scanner from collision with the component placed for scanning. Safety limits were added for FANUC S-430 IW to protect the MetraSCAN-R to avoid collision with component surface. The limits were set using the Teach Pendant of robot, by following steps: *Menus* → *System* → *Press F1* - → *select Axis Limits* → *Enter* → *change the limit angle for $J_2 = 17\text{deg}$* in the positive y-direction and $J_3 = -19$ degree in negative Z-axis direction. One can select limits based on the requirement of the application or usage.

Joint 3 (J_3) is set to limit to prevent the downwards movement in negative Z-axis direction below that set limit. Thus, a safe distance is kept between the MetraSCAN-R scanner and the component. The following message is displayed as shown in Figure 27 if the J_3 is moved in Z-axis negative direction. Similarly, joint 2 (J_2) is set as a limit angle to prevent the robot move further in the positive y-direction to avoid collision. The following message “Stroke Limit (G:1 A:2 Hex)” is displayed if a robot is jogged further than the set limit as shown in Figure 27.

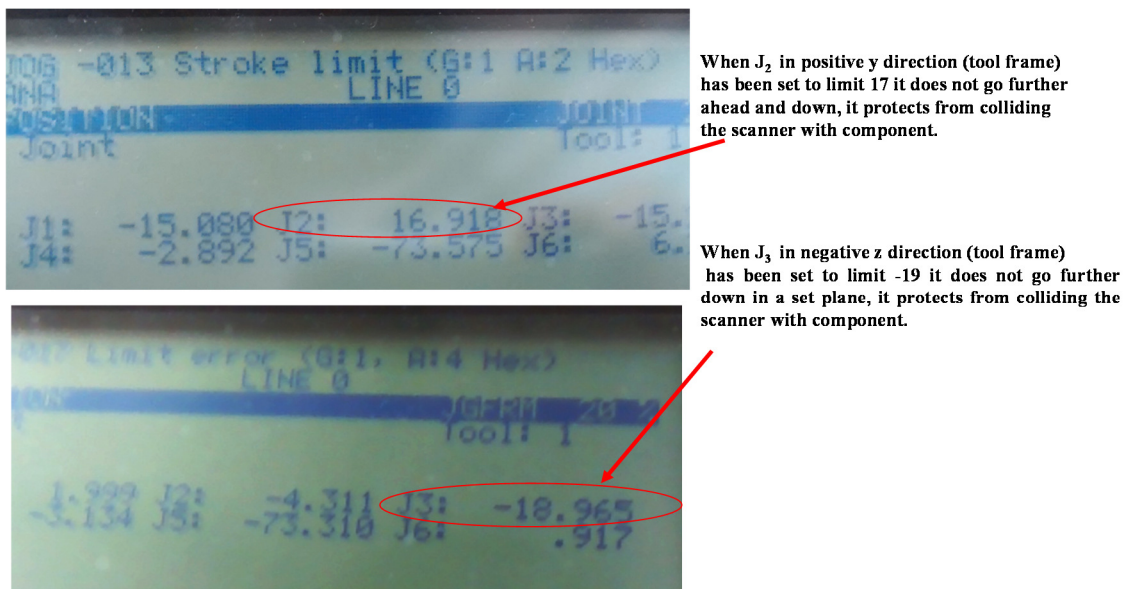


Figure 27: Setting safety limit on FANUC S-430 IW robot

6.3 Setting the Tool Frame on FANUC S-430 IW

The next task was to attach the laser scanner and beam, by assigning the tool frames for scanner and the laser beam. Tool frames 2 and 3 are used for attaching the 3D laser scanner on the robot. The z -coordinate for tool frame 1 and 2 are changed to values d_{ls} and d_{ls} plus d_{beam} . Using the Teach Pendant, this tool frame can be set initially before mounting the laser scanner MetraSCAN-R on the FANUC S-430 IW robot. On the Teach Pendant, *Menus* \rightarrow *Set-up* \rightarrow *press F1 (type)* \rightarrow *select Frames* \rightarrow *move cursor to frame 2* \rightarrow *press detail* \rightarrow *edit the z coordinate with the respective value* \rightarrow *press Enter* \rightarrow *press Prev* \rightarrow *move cursor to frame 3 and repeat the same procedure, as shown in Figure 28*

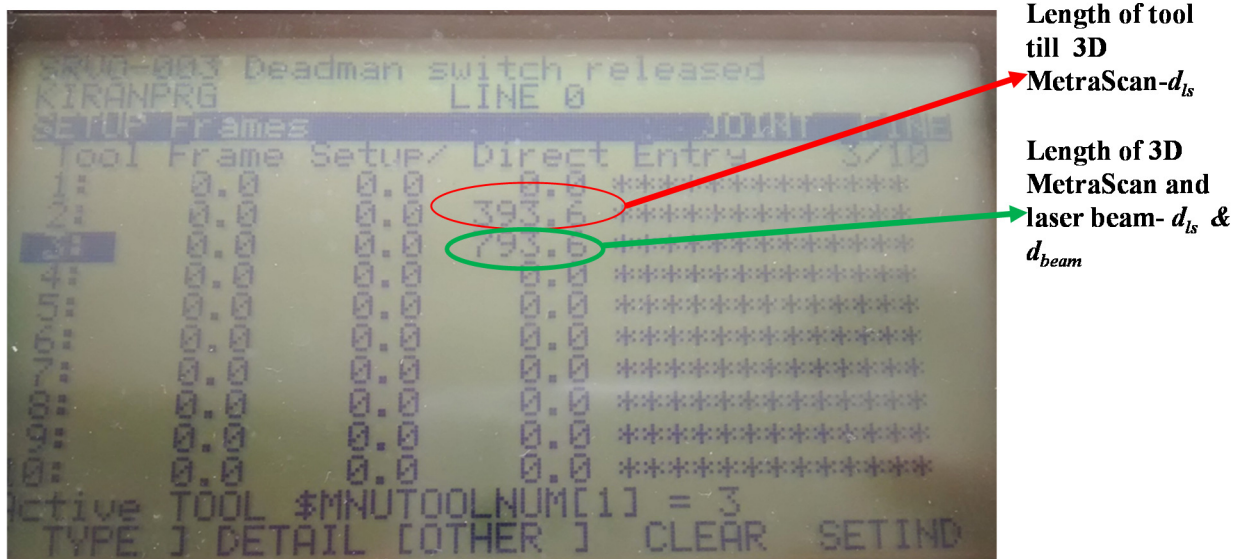


Figure 28: Setting the tool frame on the FANUC S-430 IW robot

After setting the tool frame, the MetraSCAN-R 3D scanner is mounted on the FANUC S-430 IW robot as shown in the Figure 6. As described in the procedure the laser line scanner, MetraSCAN-R is attached as a tool to the FANUC S430 IW robot and assigned to *tool frame 2* and the length of laser beam is assigned to *tool frame 3* as shown in Figure 28. The camera and scanner are calibrated initially, using the steps in the laser scanner user manual. The scanner parameters focus, resolution, view angle, and depth of view are optimized as per the instructions

for the scanner. The scanner is calibrated using the calibration plate having spherical geometric shape, as shown in Figure 29. The automatic scanner movement while scanning a surface is controlled by FANUC S430 IW using a small robot Teach Pendant program; see Appendix D.

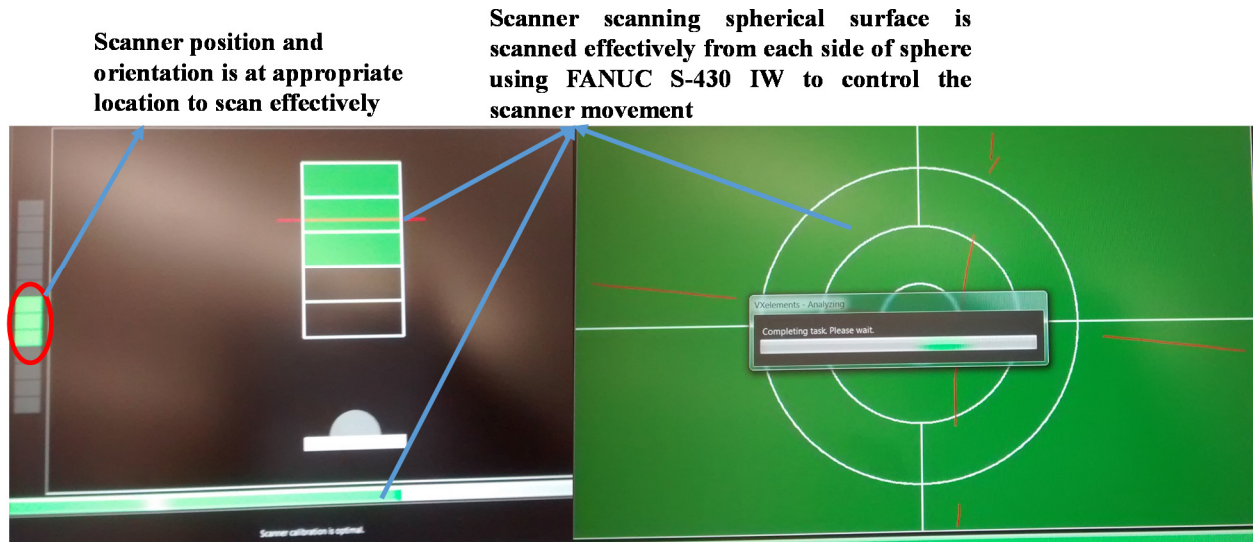


Figure 29: Scanner calibration is controlled using FANUC S430 IW robot and determined scanner position and orientation

6.4 Movement of the System Model along a Scanning Trajectory Path

In order to move the ALLS system, from its validated position to the fixed point on the trajectory of the component, the joint angles of robot θ_1 - θ_6 are calculated using the inverse kinematic equations for the FANUC S-430 IW described in Table 2 (Odeyinka 2015). From the experiment and mathematical model it has been found that θ_{ls} and θ_{beam} are equal to θ_5 as shown in Figure 30. The trajectory path was obtained using the experiment performed for scanning a spherical surface is shown in Figure 30.

The FANUC S430 IW robot movement was programmed with the Teach Pendant controls for the scanner position and orientation in relation to the spherical surface. The scanner was moved automatically to scan along the spherical surface. Thus, a trajectory path was generated by connecting all the measured points shown in Figure 30. In that scan path, at a measured point, the

joint angles are shown representing the position (x, y, z) and orientation (*Roll-Pitch-Yaw angle*) of the system with respect to the component surface. These joint angles indicate the position and orientation of the system in order for the robot to reach the component surface. In this measurement system, tool frames are set for combining the MetraSCAN-R 3D laser line scanner and its laser beam on a FANUC S430 IW robot. Validation results obtained in Figure 18 and 19 provide the relation between the FANUC S430 IW and MetraSCAN-R scanner. The result shown in Figure 20 provides the coordinates of the component surface. The calculation of joint angles shown in Figure 21 shows that this measurement system should be normal relative to the component surface point. When the system is moved from point 2 to point 4 a trajectory path is scanned. Consequently, the joint angles and actual coordinates of the system are obtained as shown in Figure 30. ALLS system moves from the validation position to the new position as described in the Figure 31. Thus, the non-contact inspection system, (FANUC S430 IW with MetraSCAN-R) acquires 'as-is' component spherical surface data, plans the trajectory path using the robot program, and obtains the kinematic relationship between the robot, scanner, and fixed component surface without an external measuring device. The objective to integrate three co-ordinate frames (the FANUC S430 IW robot, scanner, and component) while scanning a trajectory path (scan path) is achieved.

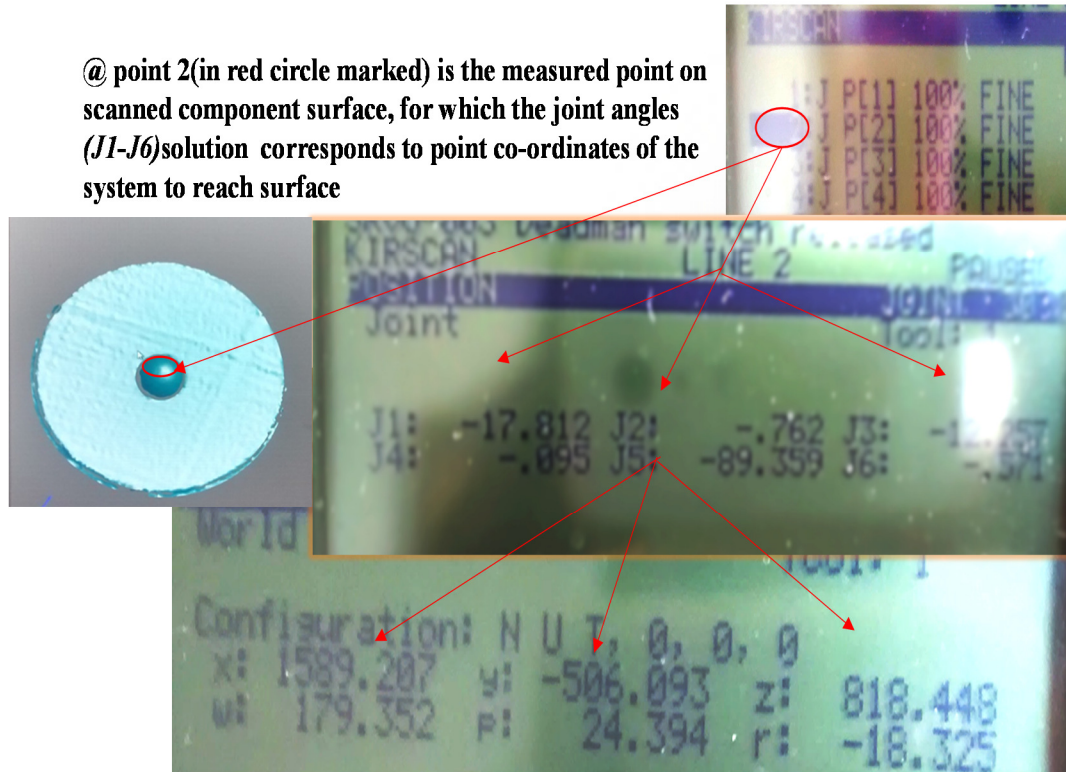


Figure 30: Scanning of Spherical surface: the position of point co-ordinates on the spherical surface and joint angles of FANUC S-430 IW robot and scanner to reach the surface.

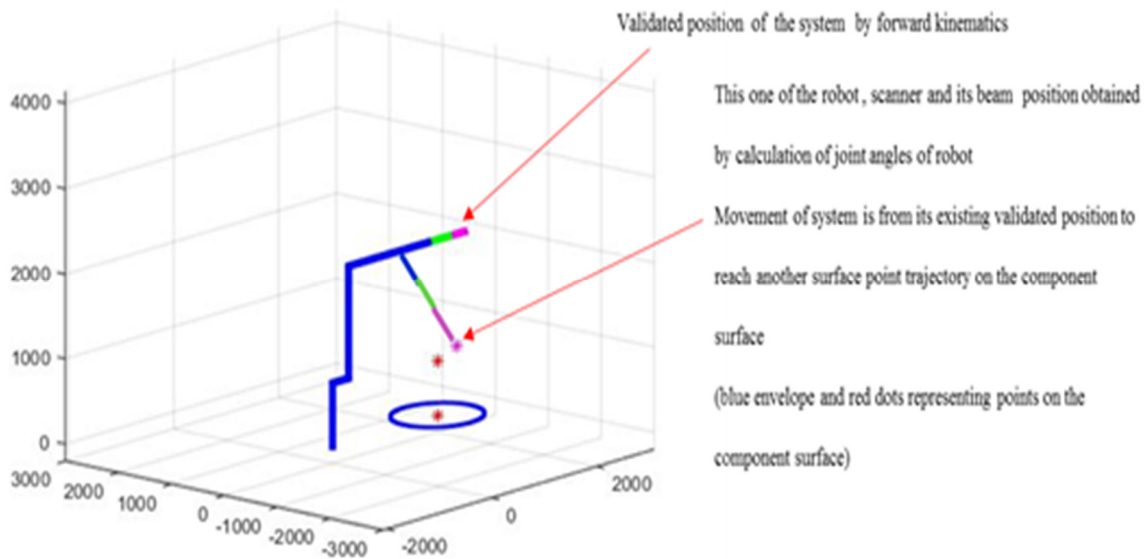


Figure 31: FANUC S430 IW Robot and MetraSCAN-R system two poses (pink dots) while scanning a trajectory points on component surface

7. CONCLUSIONS AND FUTURE WORK

The goal of this approach was to validate and determine the joint angles of the entire mechanical linkage of the ALLS system to reach the point on surface of component, as shown in Figure 30 and 31; thus, establishes a method to generate a trajectory path for laser scanning inspection. The measured points on the trajectory path corresponds to the position of the ALLS system. Each position of ALLS system represents the values of the joint angles of the FANUC S430 IW and corresponds to the measured scan point on the spherical component. The results obtained in this research provide the position and orientation coordinates of the entire measurement system along a trajectory of points on the component.

This research adds to the existing knowledge regarding the advancement of automated laser scanning systems. It contributes towards determining the kinematic relationship between the elements of the system and the component surface. The movement of the system as one mechanical linkage is called as robot pose, with obtained joint angles solutions, to reach that particular point on the component surface. This study, to the best of our knowledge, is the first to integrate all three transformations of the coordinates; from robot to laser scanner frame, laser scanner frame to laser beam frame, and laser beam to component frame. The transformation of co-ordinates from the laser beam to the component introduced in this research will play a vital role as input into future work for scan path planning and point cloud measurement prediction.

The obtained trajectory path can be the input into methods to optimize the scan path. An assumption limiting this approach is that the component surface here is sphere or circle. A change in the shape of the component would change the equation of the component surface and the point coordinates located on component. Future work would focus on any geometric shape equations for a component, and would make this mechanical linkage be able to move along the component of

any geometric shape. The obtained different position and orientation of the robot-laser scanning system can be input for future work to develop the work-window for the FANUC S430 IW robot and MetraSCAN-R scanning system.

The potential impact of this research thesis is its contribution to enhance the development of optimization methods for laser line scan paths in order to collect best point clouds. ALLS systems that can rapidly collect best point cloud datasets could become a viable inspection method in production systems and transform inspection, quality monitoring, and core condition assessment processes. Manufacturing quality monitoring systems would be provided with data and information that significantly exceeds manual inspection or traditional Coordinate Measurement Machines (CMMS). Remanufacturing condition assessment systems would benefit from an advanced system that can accurately and quickly determine the condition of an end-of-use component and develop as-is CAD models for remanufacturing planning of components.

The work of this thesis has been accepted to the 2016 North American Manufacturing Research Conference and submitted to the 2016 Proceedings for NAMRI or SME Journal of Manufacturing Systems.

APPENDIX A

MATLAB PROGRAM FOR FORWARD KINEMATICS

```

clc
clear all
%%%%%%%%%%%%%%%%%%%%%%%%%%%%%%%%%%%%%%%%%%%%%%%%%%%%%%%%%%%%%%%%%%%%%%%%
%Forward Kinematics_FANUC_S430IW
%%%%%%%%%%%%%%%%%%%%%%%%%%%%%%%%%%%%%%%%%%%%%%%%%%%%%%%%%%%%%%%%%%%%%%%%

% D-H Parameters
a1 = 305; % link offset of first arm
a2 = 1075; % link offset of second arm
a3 = -250; % link offset of third arm
a4 = 0; % link offset of fourth arm
a5 = 0; % link offset of fifth arm
a6 = 0; % link offset of sixth arm
als = 0; % width of scanner
abeam = 0; % beam center point
aw = 2438; % width of workpiece from beam centerpoint

d1 = 740; % link length of first arm
d2 = 0; % link length of second arm
d3 = 0; % link length of third arm
d4 = -1275; % link length of fourth arm
d5 = 0; % link length of fifth arm
d6 = -240; % link length of sixth arm
dls = 393.6; % length of tool and handle till laser scanner starting point
dbeam = 400; % length of laser scanner and beam
dw = 1280; % workpiece
d6b = d6 + dls + dbeam % for inverse kinematics - d6b is considered as per the geometry change as
scanner and beam are added

X = [0 0 a1 a1 a1 a1 - d4 a1 - d4 - d6]
Z = [0 d1 d1 d1 + a2 d1 + a2 - a3 d1 + a2 - a3 d1 + a2 - a3]
Y = [0 0 0 0 0 0 0]
Tool = plot3(X, Y, Z, 'b', 'LineWidth', 4)

axis([-1.5*(a1+a2) 2.25*(a1+a2) -3000 3000 -200 3*(a1+a2)])
grid on
hold('all')

ALPHA_1 = (-90*pi)/180
ALPHA_2 = (180*pi)/180
ALPHA_3 = (90*pi)/180
ALPHA_4 = (-90*pi)/180
ALPHA_5 = (90*pi)/180

```

```

ALPHA_6 = (180*pi)/180
ALPHA_1s = (0*pi)/180
ALPHA_beam = (0*pi)/180
ALPHA_wp= (0*pi)/180

```

```

theta1_0 = 0
theta2_0 = -90
theta3_0 = 180
theta4_0 = 0
theta5_0 = 0
theta6_0 = 180
thetals_0 = 0
thetabeam_0 = 0
thetawp_0 = 0

```

```

%to be input using the Teach Pendant%

```

```

theta1_Pendent = 0
theta2_Pendent = 0
theta3_Pendent = 0
theta4_Pendent = 0
theta5_Pendent = 0
theta6_Pendent = 0
thetals_Pendent = 0
thetabeam_Pendent= 0
thetawp_Pendent = 0

```

```

% conversion of joint angles to radians

```

```

theta1 = (theta1_Pendent+theta1_0)*pi/180
theta2 = (theta2_Pendent+theta2_0)*pi/180
theta3 = (theta3_Pendent+theta3_0)*pi/180
theta4 = (theta4_Pendent+theta4_0)*pi/180
theta5 = (theta5_Pendent+theta5_0)*pi/180
theta6 = (theta6_Pendent+theta6_0)*pi/180
thetals = (thetals_Pendent+thetals_0)*pi/180
thetabeam =(thetabeam_Pendent+thetabeam_0)*pi/180
thetawp = (thetawp_0+thetawp_0)*pi/180

```

```

% homogenous matrices of robot six joints represented by

```

```

%P1-P6

```

```

P1 = [cos(theta1), -cos(ALPHA_1)*sin(theta1), sin(ALPHA_1)*sin(theta1), a1*cos(theta1);
sin(theta1), cos(ALPHA_1)*cos(theta1), -sin(ALPHA_1)*cos(theta1), a1*sin(theta1); 0,
sin(ALPHA_1), cos(ALPHA_1), d1; 0, 0, 0, 1 ]
P2 = [cos(theta2), -cos(ALPHA_2)*sin(theta2), sin(ALPHA_2)*sin(theta2), a2*cos(theta2);
sin(theta2), cos(ALPHA_2)*cos(theta2), -sin(ALPHA_2)*cos(theta2), a2*sin(theta2); 0,
sin(ALPHA_2), cos(ALPHA_2), d2; 0, 0, 0, 1 ];

```

```

P3 = [cos(theta3), -cos(ALPHA_3)*sin(theta3), sin(ALPHA_3)*sin(theta3), a3*cos(theta3);
sin(theta3), cos(ALPHA_3)*cos(theta3), -sin(ALPHA_3)*cos(theta3), a3*sin(theta3); 0,
sin(ALPHA_3), cos(ALPHA_3), d3; 0, 0, 0, 1 ];
P4 = [cos(theta4), -cos(ALPHA_4)*sin(theta4), sin(ALPHA_4)*sin(theta4), a4*cos(theta4);
sin(theta4), cos(ALPHA_4)*cos(theta4), -sin(ALPHA_4)*cos(theta4), a4*sin(theta4); 0,
sin(ALPHA_4), cos(ALPHA_4), d4; 0, 0, 0, 1 ];
P5 = [cos(theta5), -cos(ALPHA_5)*sin(theta5), sin(ALPHA_5)*sin(theta5), a5*cos(theta5);
sin(theta5), cos(ALPHA_5)*cos(theta5), -sin(ALPHA_5)*cos(theta5), a5*sin(theta5); 0,
sin(ALPHA_5), cos(ALPHA_5), d5; 0, 0, 0, 1 ];
P6 = [cos(theta6), -cos(ALPHA_6)*sin(theta6), sin(ALPHA_6)*sin(theta6), a6*cos(theta6);
sin(theta6), cos(ALPHA_6)*cos(theta6), -sin(ALPHA_6)*cos(theta6), a6*sin(theta6); 0,
sin(ALPHA_6), cos(ALPHA_6), d6; 0, 0, 0, 1 ];
%% Multiplication of six homogenous matrices
P1_6 = P1*P2*P3*P4*P5*P6

%% Plot validated robot joints 1-6%%
HOME = plot3(P1_6(1,4), P1_6(2,4), P1_6(3,4), 'r*');

%% Laser scanner attached as tool or end effector
Pls= [cos(thetals), -cos(ALPHA_ls)*sin(thetals), sin(ALPHA_ls)*sin(thetals), als*cos(thetals);
sin(thetals), cos(ALPHA_ls)*cos(thetals), -sin(ALPHA_ls)*cos(thetals), als*sin(thetals); 0,
sin(ALPHA_ls), cos(ALPHA_ls), dls; 0, 0, 0, 1 ];
Pscanner= P1_6 *Pls

%% Plot laser scanner %%
Xls=[a1-d4-d6 a1-d4-d6+dls]
Zls=[d1+a2-a3 d1+a2-a3]
Yls =[0 0]
Scanner = plot3(Xls,Yls,Zls,'g','LineWidth',4)
FIRST = plot3(Pscanner(1,4), Pscanner(2,4), Pscanner(3,4), 'g*')

%%Laser beam%%
Pbeam= [cos(thetabeam), -cos(ALPHA_beam)*sin(thetabeam),
sin(ALPHA_beam)*sin(thetabeam), abeam*cos(thetabeam); sin(thetabeam),
cos(ALPHA_beam)*cos(thetabeam), -sin(ALPHA_beam)*cos(thetabeam),
abeam*sin(thetabeam); 0, sin(ALPHA_beam), cos(ALPHA_beam), dbeam; 0, 0, 0, 1 ];
Plaserb=Pscanner*Pbeam

%% Plot Laser beam %%
Xb=[a1-d4-d6+dls a1-d4-d6+dls+dbeam];
Zb=[d1+a2-a3 d1+a2-a3];
Yb =[0 0];
beam = plot3(Xb,Yb,Zb,'m','LineWidth',4)

SECOND = plot3(Plaserb(1,4), Plaserb(2,4), Plaserb(3,4), 'm*')

```

APPENDIX B

MATLAB PROGRAM FOR COMPONENT SURFACE

```
%% Plotting of component surface
```

```
r=635.8;
Px= r*cos(ALPHA_wp)*sin(thetawp);
Py= r*sin(ALPHA_wp)*sin(thetawp);
Pz= r*cos(thetawp);
X=[1 0 0 Px]
Z=[0 0 1 Pz]
Y=[0 1 0 Py]
Tool1 = plot3(X+2000,Y, Z, 'r*')

for i= 0:180
    d = i *pi/180
    for ALPHA_w = 0:d:180;
        for beta_w = 0:d:180;

            Pw =[cos(ALPHA_w)*cos(beta_w), -sin(ALPHA_w), cos(ALPHA_w)*sin(beta_w), r*
cos(ALPHA_w)* sin(beta_w); sin(ALPHA_w)*cos(beta_w), cos(ALPHA_w),
sin(ALPHA_w)*sin(beta_w), r*sin(ALPHA_w)*sin(beta_w); -sin(beta_w), 0,
cos(beta_w),r*cos(beta_w); 0,0,0,1];
Envelope_1 = plot(Pw(1,4)+2000,Pw(3,4), 'b.')
refreshdata(Tool1,'caller')
drawnow
pause(.1)
        end
    end
end
```

APPENDIX C

MATLAB PROGRAM FOR INVERSE KINEMATICS

```

%%Inverse kinematics
%% Using Samuel inverse kinematics for Fanuc family of robot for our FANUC S430 IW robot
%%

px6=P1_6(1,4)
py6=P1_6(2,4)
pz6=P1_6(3,4)

ax= P1_6(1,3)
ay=P1_6(2,3)
az=P1_6(3,3)
a=[ ax, ay, az]
px =px6 -abs(d6)*a(1,1)
py=py6-abs(d6)*a(1,2)
pz=pz6-abs(d6)*a(1,3)

%T4= P1*P2*P3*P4
%Px=T4(1,4)
%Py=T4(2, 4)
%Pz=T4(3,4)
z0=[1 0 0]
ARM=sign(dot(a,z0))
THETA1 = (atan2( Py,(ARM*Px)))*180/pi
THETA1= THETA1+180

% Joint solution 2
r= sqrt(PX^2+py^2)-(a1*ARM)
R = sqrt(r^2+(pz- abs(d1))^2)
cos_betha=((a2)^2+R^2-(a3)^2-(d4)^2)/(2*R*(a2))
sin_betha=sqrt(1-(cos_betha)^2)
sin_fi=-pz-abs(d1)/R
cos_fi=-(r/R)*ARM
ELBOW = ARM*sign(-d4*cos(theta3_Pendent)+a3*sin(theta3_Pendent))
sin_THETA2 = (sin_fi*cos_betha+ARM*ELBOW*cos_fi*sin_betha)
cos_THETA2 = (cos_fi*cos_betha-ARM*ELBOW*sin_fi*sin_betha)
THETA2 = (atan2(sin_THETA2,cos_THETA2)*180)/pi
THETA2 = theta2_0 - (atan2(sin_THETA2,cos_THETA2)*180/pi)
THETA2 = theta2_0 + (atan2(sin_THETA2,cos_THETA2)*180/pi)

A4=P3*P4
E= A4(2,4)
ELBOW=ARM*sign (A4(2,4))

```

```
% joint 3
```

```
cos_fi=((a2)^2+(a3)^2+(d4)^2-(R)^2)/(2*(a2)*sqrt((a3)^2+(d4)^2))
sin_fi=ARM*ELBOW*sqrt(1-(cos_fi)^2)
sin_betha=abs(d4)/sqrt((a3)^2+(d4)^2)
cos_betha=abs(a3)/sqrt((a3)^2+(d4)^2)
sin_THETA3= cos_fi*sin_betha-sin_fi*cos_betha
cos_THETA3= cos_fi*cos_betha+sin_fi*sin_betha
THETA3=((atan2(sin_THETA3,cos_THETA3)*180)/pi)
THETA3_deg=THETA3-theta3_0
THETA3_deg=THETA3+theta3_0
```

```
% joint 4 solution
```

```
H=P1*P2*P3
X3=H(1:3,1)
y3=H(1:3,2)
Z3=H(1:3,3)
F3=H(1:3,4)
a=transpose(a)
Z4=(cross(Z3,a))
sin_THETA4=-((dot(Z4,X3)))
cos_THETA4=(dot(Z4,y3))
THETA4= ((atan2(sin_THETA4,cos_THETA4)*180)/pi)
THETA4= THETA4+180
THETA4= THETA4-90
THETA4= 90-((atan2(sin_THETA4,cos_THETA4)*180)/pi)
THETA4= THETA4-180
```

```
% Derivation of Wrist configuration
```

```
Z5=-a
y5=Z4
S=-y5
WRIST= sign(dot(S,Z4))
```

```
%% joint 5 solution
```

```
q1= P1*P2*P3*P4
nx=q1(1,1)
ny=q1(2,1)
nz=q1(3,1)
n=[nx ny nz] % vector representing in x4 direction
X4=transpose(n)

sx=q1(1,2)
sy=q1(2,2)
sz=q1(3,2)
s=[sx sy sz] % vector representing in y4 direction
Y4= transpose(s)
```

```

ax=q1(1,3)
ay=q1(2,3)
az=q1(3,3)
a=[ax,ay,az] % vector representing in z4 direction
a=transpose(a)

sin_THETA5= dot(-a, X4)
cos_THETA5= dot(-a, Y4)
THETA5=((atan2(sin_THETA5,cos_THETA5)*180)/pi)
THETA5=180- ((atan2(sin_THETA5,cos_THETA5)*180)/pi) % joint 5 solution
THETA5=-THETA5
THETA5=THETA5+270
THETA5=THETA5-270

% Joint 6 solution
q2= P1*P2*P3*P4*P5
nx=q2(1,1)
ny=q2(2,1)
nz=q2(3,1)
n=[nx ny nz] % vector representing in x4 direction
X5=transpose(n)

sx=q2(1,2)
sy=q2(2,2)
sz=q2(3,2)
s=[sx sy sz] % vector representing in y4 direction
Y5= transpose(s)

sin_THETA6= dot(n,Y5)
cos_THETA6= dot(s,-Y5)
THETA6= ((atan2(sin_THETA6,cos_THETA6)*180)/pi) % Joint 6 solution
THETA6= THETA6 + pi % when flip toggle is 1 or on
% plotting of robot, scanner and beam again after calculating joint angles
X=[0 0 a1 a1 a1-d4 a1-d4-d6b]
Z=[0 d1 d1 d1+a2 d1+a2-a3 d1+a2-a3 d1+a2-a3]
Y=[0 0 0 0 0 0]
Tool = plot3(X,Y,Z,'b','LineWidth',4)

axis([-1.5*(a1+a2) 2.25*(a1+a2) -3000 3000 -200 3*(a1+a2)])
grid on
hold('all')

P1 = [cos(THETA1), -cos(ALPHA_1)*sin(THETA1), sin(ALPHA_1)*sin(THETA1),
a1*cos(THETA1); sin(THETA1), cos(ALPHA_1)*cos(THETA1), -
sin(ALPHA_1)*cos(THETA1), a1*sin(THETA1); 0, sin(ALPHA_1), cos(ALPHA_1), d1; 0, 0,
0, 1 ]

```

```
P2 = [cos(THETA2), -cos(ALPHA_2)*sin(THETA2), sin(ALPHA_2)*sin(THETA2),
a2*cos(THETA2); sin(THETA2), cos(ALPHA_2)*cos(THETA2), -
sin(ALPHA_2)*cos(THETA2), a2*sin(THETA2); 0, sin(ALPHA_2), cos(ALPHA_2), d2; 0, 0,
0, 1 ]
```

```
P3 = [cos(THETA3), -cos(ALPHA_3)*sin(THETA3), sin(ALPHA_3)*sin(THETA3),
a3*cos(THETA3); sin(THETA3), cos(ALPHA_3)*cos(THETA3), -
sin(ALPHA_3)*cos(THETA3), a3*sin(THETA3); 0, sin(ALPHA_3), cos(ALPHA_3), d3; 0, 0,
0, 1 ]
```

```
P4 = [cos(THETA4), -cos(ALPHA_4)*sin(THETA4), sin(ALPHA_4)*sin(THETA4),
a4*cos(THETA4); sin(THETA4), cos(ALPHA_4)*cos(THETA4), -
sin(ALPHA_4)*cos(THETA4), a4*sin(THETA4); 0, sin(ALPHA_4), cos(ALPHA_4), d4; 0, 0,
0, 1 ]
```

```
P5 = [cos(THETA5), -cos(ALPHA_5)*sin(THETA5), sin(ALPHA_5)*sin(THETA5),
a5*cos(THETA5); sin(THETA5), cos(ALPHA_5)*cos(THETA5), -
sin(ALPHA_5)*cos(THETA5), a5*sin(THETA5); 0, sin(ALPHA_5), cos(ALPHA_5), d5; 0, 0,
0, 1 ]
```

```
P6 = [cos(THETA6), -cos(ALPHA_6)*sin(THETA6), sin(ALPHA_6)*sin(THETA6),
a6*cos(THETA6); sin(THETA6), cos(ALPHA_6)*cos(THETA6), -
sin(ALPHA_6)*cos(THETA6), a6*sin(THETA6); 0, sin(ALPHA_6), cos(ALPHA_6), d6; 0, 0,
0, 1 ]
```

```
%% Multiplication of six homogenous matrices
```

```
P1_6 = P1*P2*P3*P4*P5*P6
```

```
%% Plot validated robot joints 1-6
```

```
HOME = plot3(P1_6(1,4), P1_6(2,4), P1_6(3,4), 'r');
```

```
%% Laser scanner attached as tool or end effector
```

```
Pls= [cos(thetals), -cos(ALPHA_ls)*sin(thetals), sin(ALPHA_ls)*sin(thetals), als*cos(thetals);
sin(thetals), cos(ALPHA_ls)*cos(thetals), -sin(ALPHA_ls)*cos(thetals), als*sin(thetals); 0,
sin(ALPHA_ls), cos(ALPHA_ls), dls; 0, 0, 0, 1 ];
```

```
Pscanner= P1_6 *Pls
```

```
%% Plot laser scanner
```

```
Xls=[a1-d4-d6 a1-d4-d6+dls]
```

```
Zls=[d1+a2-a3 d1+a2-a3]
```

```
Yls =[0 0]
```

```
Scanner = plot3(Xls,Yls,Zls,'g','LineWidth',4)
```

```
FIRST = plot3(Pscanner(1,4), Pscanner(2,4), Pscanner(3,4), 'r')
```

```
%% Laser beam
```

```
Pbeam= [cos(thetabeam), -cos(ALPHA_beam)*sin(thetabeam),
sin(ALPHA_beam)*sin(thetabeam), abeam*cos(thetabeam); sin(thetabeam),
cos(ALPHA_beam)*cos(thetabeam), -sin(ALPHA_beam)*cos(thetabeam),
abeam*sin(thetabeam); 0, sin(ALPHA_beam), cos(ALPHA_beam), dbeam; 0, 0, 0, 1 ];
```

```
Plaserb=Pscanner*Pbeam
```

```
%% Plot Laser beam %%
```

```
Xb=[a1-d4-d6+dls a1-d4-d6+dls+dbeam];
```

```
Zb=[d1+a2-a3 d1+a2-a3];
```

```
Yb =[0 0];
```

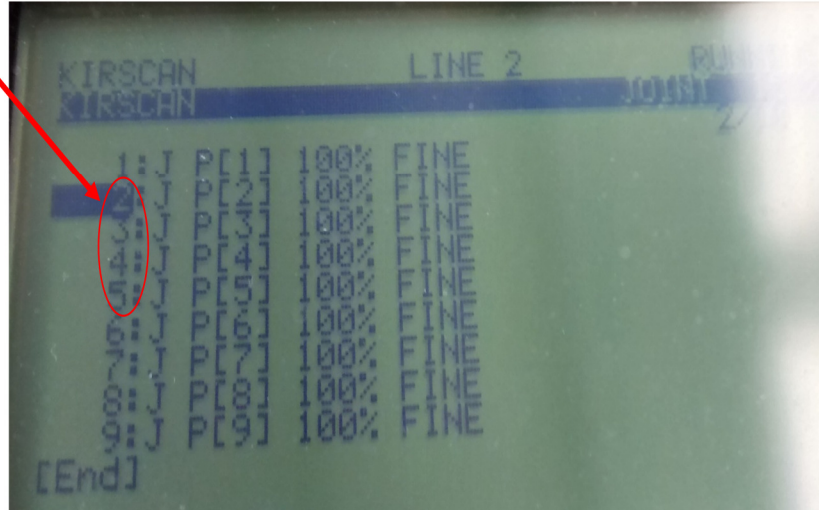
```
beam = plot3(Xb,Yb,Zb,'m','LineWidth', 4)
```

```
SECOND = plot3(Plaserb(1,4), Plaserb(2,4), Plaserb(3,4), 'm*')
```

APPENDIX D

TEACH PENDENT PROGRAM TO SCAN A TRAJECTORY POINTS ON SPHERICAL SURFACE

Trajectory path
points on sphere
surface-calibration
plate



REFERENCES

- Arachchige, P., Abderrahmane, M., & Djuric, A. M. Modeling and Validation of Rapid Prototyping Related Available Workspace. *SAE International Journal of Materials and Manufacturing*, 2014, 7, 291-299.
- Bračun, D., Jezeršek, M., & Diaci, J. Triangulation Model Taking into Account Light Sheet Curvature. *Measurement Science and Technology*, 2006, 17:2191.
- Borangiu, T., Dogar, A., & Dumitrache, A. A heuristic approach for constrained real time motion planning of a redundant 7-dof mechanism for 3D laser scanning. Paper presented at the Information Control Problems in Manufacturing. 13th IFAC Symp. on Information Control Problems in Manufacturing-INCOM,2009.
- Buchsbaum, F., & Freudenstein, F. Synthesis of kinematic structure of geared kinematic chains and other mechanisms. *Journal of mechanisms*, 1970, 5(3), 357-392.
- Chen, C., Wang, Y., Ou, H., He, Y., & Tang, X. A review on remanufacture of dies and moulds. *Journal of Cleaner Production*, 2014, 64,13-23.
- Chow, J. Reproducing aircraft structural components using laser scanning. *The International Journal of Advanced Manufacturing Technology*, 1997, 13(10), 723-728.
- Decker, S. Dynamic Measurement of Position and Orientation of Robots. *Instrumentation and Measurement Technology Conference*, 1992, 9th IEEE, 1990, 300-304
- Denavit, J. A kinematic notation for lower-pair mechanisms based on matrices. *Trans. of the ASME. Journal of Applied Mechanics*, 1955, 22, 215-221.
- Denavit, R. Hartenberg. A Kinematic Notation for Lower-Pair Mechanisms Based on Matrices. *ASME Journal*, 1955, 215-221.

- Derigent, W., Chapotot, E., Ris, G., Remy, S., & Bernard. 3D digitizing strategy planning approach based on a CAD model. *Journal of computing and information science in engineering*, 2007, 7(1), 10-19.
- Djuric, A., & Urbanic, R. A Methodology for Defining the Functional Space (Work Window) for a Machine Configuration. Paper presented at the 3rd International Conference on Changeable, Agile, Reconfigurable and Virtual Production, 2009.
- Dornaika, F., & Horaud, R. Simultaneous robot-world and hand-eye calibration. *Robotics and Automation, IEEE Transactions on*, 1998, 14(4), 617-622.
- Durupt, A., Remy, S., Ducellier, G., & Eynard, B. From a 3D point cloud to an engineering CAD model: a knowledge-product-based approach for reverse engineering. *Virtual and Physical Prototyping*, 2008, 3(2), 51-59.
- ElMaraghy, H. & Yang, X. Computer-aided Planning of Laser Scanning of Complex Geometries. *CIRP Annals-Manufacturing Technology*, 2003, 52(1):411-414.
- FANUC America Corporation Quick Reference Document
- Feng, H.-Y., Liu, Y., & Xi, F. Analysis of digitizing errors of a laser scanning system. *Precision Engineering*, 2001, 25(3), 185-191
- Fernández, P., Rico, J. C., Álvarez, B. J., Valiño, G., & Mateos, S. Laser scan planning based on visibility analysis and space partitioning techniques. *The International Journal of Advanced Manufacturing Technology*, 2008, 39(7-8), 699-715.
- Fu, K. S., Gonzalez, R., & Lee, C. G. *Robotics: Control Sensing. Vis*: Tata McGraw-Hill Education, 1987.

- Haapala, K. R., Zhao, F., Camelio, J., Sutherland, J. W., Skerlos, S. J., Dornfeld, D. A., . . . Rickli, J. L. A review of engineering research in sustainable manufacturing. *Journal of manufacturing science and engineering*, 2013, 135(4), 041013.
- Jin, X., & Yang, X. Off-line Programming of a Robot for Laser Re-manufacturing. *Tsinghua Science & Technology*, 2009, 14(s1):186-191.
- Kashani, A., Owen, W. S., Himmelman, N., Lawrence, P. D., & Hall, R. A. Laser Scanner-based End-effector Tracking and Joint Variable Extraction for Heavy Machinery. *The International Journal of Robotics Research*, 2010.
- Kim, C., Espalin, D., Cuaron, A., Perez, M. A., Lee, M., MacDonald, E., & Wicker, R. B. Cooperative Tool Path Planning for Wire Embedding on Additively Manufactured Curved Surfaces Using Robot Kinematics. *Journal of Mechanisms and Robotics*, 2015, 7(2), 021003.
- Kriegel, S., Bodenmüller, T., Suppa, M., & Hirzinger, G. A surface-based next-best-view approach for automated 3D model completion of unknown objects. Paper presented at the Robotics and Automation (ICRA), 2011 IEEE International Conference on., 2011
- Kuş, A. Implementation of 3D optical scanning technology for automotive applications. *Sensors*, 2009, 9(3), 1967-1979.
- Larsson, S. & Kjellander, J. Motion Control and Data Capturing for Laser Scanning with an Industrial Robot. *Robotics and Autonomous Systems*, 2006, 54(6):453-460.
- Larsson, S. & Kjellander, J. A. Path Planning for Laser Scanning with an Industrial Robot. *Robotics and Autonomous Systems*, 2008, 56(7):615-624.
- Lee, K. H., & Park, H.P. Automated Inspection Planning of Free-Form Shape Parts by Laser scanning. *Robotics and Computer-Integrated Manufacturing*, 2000, 16(4):201-210.

- Lee, C.S.G, & Ziegler M. A Geometric Approach in Solving The Inverse Kinematics of PUMA Robots. Ann Arbor, Michigan, December 1983.
- Leigh-Lancaster, C., Shirinzadeh, B. & Koh, Y. Development of a Laser Tracking System. Mechatronics and Machine Vision in Practice, 1997. Proceedings., Fourth Annual Conference on, 1997. IEEE, 163-168.
- Lu, F., & Milios, E. Robot pose estimation in unknown environments by matching 2d range scans. Journal of Intelligent and Robotic Systems, 1997,18(3), 249-275.
- Mayer, J. R., & Parker. A portable instrument for 3-D dynamic robot measurements using triangulation and laser tracking. Robotics and Automation, IEEE Transactions on, 1994, 10(4), 504-516.
- Manocha, D., & Canny, J. F. Efficient inverse kinematics for general 6R manipulators. Robotics and Automation, IEEE Transactions on, 1994, 10(5), 648-657.
- Mehdi-Souzani, C., Thiébaud, F., & Lartigue, C. Scan planning strategy for a general digitized surface. Journal of computing and information science in engineering, 2006, 6(4), 331-339.
- Norman, A. R., Schonberg, A., Gorchach, I. A. & Schitt, R. Validation of Igps as an External Measurement System for Cooperative Robot Positioning. The International Journal of Advanced Manufacturing Technology, 2013, 64.1-4: 427-46.
- Odeyinka, S. M. Complete Geometrical Approach to the Solution of Inverse Kinematics of FANUC 6DOF Robot Families., Master Thesis, Wayne State University, 2015, 1-64.
- Odeyinka, S. M., & Djuric, A. M. Fanuc Family Inverse Kinematics Modeling, Validation and Visualization, 2016 (0148-7191).
- Pieper, D. The kinematics of manipulators under computer control. PhD diss. Mechanical Engineering Dept., Stanford Univ, 1968.

- Pauly, M., Mitra, N. J., & Guibas, L. J. Uncertainty and Variability in Point Cloud Surface Data. Symposium on Point-based Graphics, 2004, 9.
- Papaioannou, G., Karabassi, E.-A., & Theoharis, T. Reconstruction of three-dimensional objects through matching of their parts. Pattern Analysis and Machine Intelligence, IEEE Transactions on, 2002 24(1), 114-124.
- Paoli, A., & Rationale, A. V. Large yacht hull measurement by integrating optical scanning with mechanical tracking-based methodologies. Robotics and Computer-Integrated Manufacturing, 2012, 28(5), 592-601.
- Rickli, J. L., Dasgupta, A. K., & Dinda, G. P. A descriptive framework for additive Remanufacturing systems. International Journal of Rapid Manufacturing, 2014, 4(2-4), 199-218.
- Reinhart, G. & Tekouo, W. Automatic Programming of Robot-mounted 3D Optical Scanning Devices to Easily Measure Parts in High-variant Assembly. CIRP Annals-Manufacturing Technology, 2009, 58(1): 25-28.
- Santolaria, J., Guillomía, D., Cajal, C., Albajez, J. A., & Aguilar, J. J. Modelling and calibration technique of laser triangulation sensors for integration in robot arms and articulated arm coordinate measuring machines. Sensors, 2009, 9(9), 7374-7396.
- Shiu, Y. C., & Ahmad, S. Calibration of wrist-mounted robotic sensors by solving homogeneous transform equations of the form $AX = XB$. Robotics and Automation, IEEE Transactions on, 1989, 5(1), 16-29.
- Shen, C. & Zhu, S. A Robotic System for Surface Measurement Via 3D Laser Scanner. In Proceedngs of the 2nd International Conference on Computer Applications and System Modeling, 2012, 21, Paris, France. Atlantis Press.

- Son, S., Park, H., & Lee, K. H. Automated Laser Scanning System for Reverse Engineering and Inspection. *International Journal of Machine Tools and Manufacture*, 2002, 42(8): 889-897.
- Surmann, H., Nüchter, A., & Hertzberg, J. (2003). An autonomous mobile robot with a 3D laser range finder for 3D exploration and digitalization of indoor environments. *Robotics and Autonomous Systems*, 2003, 45(3), 181-198.
- Stamos, I., & Leordean, M. Automated feature-based range registration of urban scenes of large scale. Paper presented at the Computer Vision and Pattern Recognition, 2003. Proceedings. 2003 IEEE Computer Society Conference on.
- Triebel, R., Frank, B., Meyer, J., & Burgard, W. First Steps Towards a Robotic System for Flexible Volumetric Mapping of Indoor Environments. *Proc. of the 5th IFAC Symp. on Intelligent Autonomous Vehicles*, 2004.
- Vincze, M., Prenninger, J. P., & Gander, H. A Laser Tracking System to Measure Position and Orientation of Robot End Effectors Under Motion. *The International Journal of Robotics Research*, 1994, 13.4: 305-314
- Wu, X., & Hu, Y. An Optical Scanner Aided Flexible Restoration System. Paper presented at the Intelligent System Design and Engineering Application (ISDEA), 2012 Second International Conference on., 2012.
- Wang, Z., Mastrogiacomo, L., Franceschini, F., & Maropoulos, P. Experimental comparison of dynamic tracking performance of iGPS and laser tracker. *The International Journal of Advanced Manufacturing Technology*, 2011, 56(1-4), 205-213.
- Xi, F. & Shu, C. CAD-based path planning for 3-D line laser scanning. *Computer-Aided Design*, 1999, 31:7, 473-479.

- Yin, S., Ren, Y., Guo, Y., Zhu, J., Yang, S., & Ye, S. Development and Calibration of an Integrated 3D Scanning System for High-accuracy Large-scale Metrology. *Measurement*, 2014, 54: 65-76.
- Yau, H-T., & Menq, C-H. Automated CMM path planning for dimensional inspection of dies and molds having complex surfaces. *International Journal of Machine Tools and Manufacture*, 1995, 35:6, 861-876.
- Zheng, J., Li, Z., & Chen, X. Worn area modeling for automating the repair of turbine blades. *The International Journal of Advanced Manufacturing Technology*, 2006, 29(9-10), 1062-1067.
- Zhu, S., Guo, Y.-c., & Yang, P. Remanufacturing system based on totally automatic MIG surfacing via robot. *Journal of Central South University of Technology*, 2005, 12(2), 129-132.
- Zhu, S., Cui, P.-z., Shen, C.-d., & Guo, Y.-c. Scanner external calibration algorithm based on fixed point in robot remanufacturing system. *Journal of Central South University of Technology*, 2005, 12(2), 133-137.
- Zheng, W., Luca, M., Paul, M. & Fiorenzo, F. Experimental Comparison of Dynamic Tracking Performance of iGPS and Laser Tracker. *The International Journal of Advanced Manufacturing Technology*, 2011, 56.1-4: 205-13.

ABSTRACT**KINEMATIC MODELING OF AN AUTOMATED LASER LINE SCANNING SYSTEM**

by

KIRAN SUNIL DESHMUKH**May 2016****Advisor:** Dr. Jeremy Rickli**Major:** Engineering Management**Degree:** Master of Science

This research work describes the geometric coordinate transformation in an automated laser line scanning system caused by movements required for scanning a component surface. The elements of an automated laser scanning system (robot, laser line scanner, and the component coordinate system) function as a mechanical linkage to obtain a trajectory on a component surface. This methodology solves the forward kinematics, derives the component surface, and uses inverse kinematic equations to characterize the movement of the entire automated scanning system on point trajectory. To reach a point on the component, joint angles of robot have been calculated. As a result, trajectory path is obtained. This obtained robot poses on point trajectory of the component surface can be used as an input for future work that aims to develop optimal scan paths to collect “best” point cloud datasets. This work contributes in laser scanning inspection of component surfaces in manufacturing, remanufacturing, and reverse engineering applications.

AUTOBIOGRAPHICAL STATEMENT

I am Kiran Deshmukh, a graduate student in Engineering Management at Wayne State University. I received my bachelor's degree in Instrumentation and Control Engineering at the University of Pune, India. I have worked in the manufacturing industry for a few years. I was motivated by the research work of Dr. Jeremy L. Rickli to pursue this thesis work. During the past two years, I developed expertise in Robotics and Matlab modeling. The work of this thesis has and acceptance to the 2016 North American Manufacturing Research Conference (NAMRC). My research has boosted my confidence and gives me the entry opportunity into the research area of kinematics and remanufacturing. This work will help in my future jobs involving Matlab, and in Quality Engineering and Industrial Automation. *The work of this thesis has been accepted to the 2016 North American Manufacturing Research Conference and will be submitted to the SME Journal of Manufacturing Systems.*